



# Tob Regulates the Timing of Sleep Onset at Night in *Drosophila*

Emily Han,<sup>1\*</sup> Sang Soo Lee,<sup>2\*</sup> Kristen H. Park,<sup>2</sup> Ian D. Blum,<sup>2</sup>  Qiang Liu,<sup>2</sup> Anuradha Mehta,<sup>2</sup> Isabelle Palmer,<sup>2</sup> Habon Issa,<sup>2</sup> Alice Han,<sup>2</sup> Matt P. Brown,<sup>1</sup> Victor M. Sanchez-Franco,<sup>3</sup> Miguel Velasco,<sup>2</sup> Masashi Tabuchi,<sup>3</sup> and  Mark N. Wu<sup>1,2</sup>

<sup>1</sup>Solomon H. Snyder Department of Neuroscience, Johns Hopkins University, Baltimore, Maryland 21205, <sup>2</sup>Department of Neurology, Johns Hopkins University, Baltimore, Maryland 21205, and <sup>3</sup>Department of Neurosciences, Case Western Reserve University, Cleveland, Ohio 44106

Sleep is regulated by homeostatic sleep drive and the circadian clock. While tremendous progress has been made in elucidating the molecular components of the core circadian oscillator, the output mechanisms by which this robust oscillator generates rhythmic sleep behavior remain poorly understood. At the cellular level, growing evidence suggests that subcircuits in the master circadian pacemaker suprachiasmatic nucleus (SCN) in mammals and in the clock network in *Drosophila* regulate distinct aspects of sleep. Thus, to identify novel molecules regulating the circadian timing of sleep, we conducted a large-scale screen of mouse SCN-enriched genes in *Drosophila*. Here, we show that Tob (Transducer of ERB-B2) regulates the timing of sleep onset at night in female fruit flies. Knockdown of Tob pan-neuronally, either constitutively or conditionally, advances sleep onset at night. We show that Tob is specifically required in “evening neurons” (the LNDs and the fifth s-LNV) of the clock network for proper timing of sleep onset. Tob levels cycle in a clock-dependent manner in these neurons. Silencing of these “evening” clock neurons results in an advanced sleep onset at night, similar to that seen with Tob knockdown. Finally, sharp intracellular recordings demonstrate that the amplitude and kinetics of LND postsynaptic potentials (PSPs) cycle between day and night, and this cycling is attenuated with Tob knockdown in these cells. Our data suggest that Tob acts as a clock output molecule in a subset of clock neurons to potentiate their activity in the evening and enable the proper timing of sleep onset at night.

**Key words:** circadian; clock neuron; *Drosophila*; screen; SCN; sleep

## Significance Statement

Well-timed, high-quality sleep is critical for human health and function. Elucidating how sleep is regulated by the circadian clock may reveal molecular targets for intervening in this process. However, our understanding of the genetic mechanisms underlying clock regulation of sleep is limited. From a high-throughput behavioral screen in *Drosophila*, we identified a novel clock output gene *tob* (*transducer of erb-b2*) required for proper timing of sleep onset at night. Tob levels cycle under clock control, and we show that Tob facilitates postsynaptic potentiation in a specific population of clock neurons. Our work suggests a molecular mechanism by which the clock regulates sleep onset by potentiating the function of a subset of clock neurons at night.

## Introduction

Sleep, an essential process conserved throughout the animal kingdom, is regulated by two main mechanisms: the circadian clock and homeostatic drive (Allada and Siegel, 2008; Borbély et al., 2016; Keene and Duboue, 2018). Properly timed sleep has been increasingly recognized for its importance in human

health, due to its roles in metabolism, memory, mood, immunity, and aging (Lavie, 2001; Dijk and Lockley, 2002; Jagannath et al., 2013, 2017; Irish et al., 2015). Differences in chronotypes and social- or work-related factors can result in misalignment of sleep timing with the day/night cycle, leading to suboptimal sleep. However, the molecular and cellular

Received March 2, 2023; revised Feb. 26, 2024; accepted Feb. 29, 2024.

Author contributions: E.H., S.S.L., I.D.B., M.T., and M.N.W. designed research; E.H., S.S.L., K.H.P., I.D.B., Q.L., A.M., I.P., H.L., A.H., M.P.B., V.M.S.-F., M.V., and M.T. performed research; E.H., S.S.L., K.H.P., I.D.B., A.M., M.P.B., V.M.S.-F., and M.T. analyzed data.

We thank K. Si and G. Rubin for kindly sharing reagents. We thank J.L. Bedont and S. Blakshaw for sharing unpublished results. We thank W. Joiner, the Developmental Studies Hybridoma Bank, Allen Brain Institute and Flybase for Sleeplab, antibodies, and gene-related data, respectively. We also thank the Bloomington Stock Center [supported by National Institutes of Health (NIH) grant P400D018537], the Vienna *Drosophila* Stock Center (<http://stockcenter.vdrc.at/>),

and the TRiP at Harvard Medical School (supported by NIH grant R01GM084947) for fly stocks used in this study. We thank members of the Wu lab for discussion. This work was supported by NIH grants 5F31NS117175 (M.P.B.), K99NS101065, R01NS101065 (M.T.), R35GM142490 (M.T.), R35NS122181 (M.N.W.), and R01NS079584 (M.N.W.).

\*E.H. and S.S.L. contributed equally to this work.

The authors declare no competing financial interests.

Correspondence should be addressed to Mark N. Wu at [marknwu@jhmi.edu](mailto:marknwu@jhmi.edu).

<https://doi.org/10.1523/JNEUROSCI.0389-23.2024>

Copyright © 2024 the authors

mechanisms underlying the circadian control of sleep timing remain poorly understood.

In mammals, the suprachiasmatic nucleus (SCN) is the dominant circadian pacemaker, regulating the timing of sleep–wake cycle, among other important physiological functions (Mistlberger, 2005; Takahashi et al., 2008; Welsh et al., 2010; Herzog et al., 2017; Sanchez and de la Iglesia, 2021; Sanchez et al., 2022). Brain structures important for sleep timing such as the ventrolateral preoptic nucleus, the lateral hypothalamus, and the pineal gland largely receive indirect projections from the SCN (Kalsbeek et al., 2006). In addition to synaptic connections, SCN neurons also secrete factors such as Prokineticin 2 (Prok2) that regulate sleep timing (Cheng et al., 2002). Interestingly, recent research has revealed that distinct neurons in the SCN can shape specific features of sleep. Specifically, vasoactive intestinal polypeptide (VIP) expressing neurons in the SCN have been found to regulate the night time “siesta” in mice (Collins et al., 2020).

The *Drosophila* circadian timing system, a network of ~150 clock neurons, shares remarkable similarities with the SCN: a network of multiple independent but coupled subpopulations of oscillating neurons, synchronized by neuropeptide signaling and featuring strong cycling of conserved core clock genes. Both *Drosophila* and mammalian clock networks receive light input and project to sleep/arousal centers to regulate the timing of sleep (Allada and Siegel, 2008; Allada and Chung, 2010; Welsh et al., 2010; Dubowy and Sehgal, 2017). These commonalities make *Drosophila* a useful model for studying the principles governing circadian network activity and identifying the mechanisms by which clock neurons regulate sleep.

While decades of research have delineated the molecular mechanisms underlying the core clock, the molecular pathways by which this core clock regulates sleep timing remain poorly understood. Because sleep and circadian behaviors are highly conserved across the animal kingdom, often with analogous molecular and circuit mechanisms, we hypothesized that additional studies in *Drosophila* would help elucidate conserved molecular mechanisms mediating the circadian regulation of sleep. Here, we combine the power of *Drosophila* genetics and our knowledge of genes expressed in the mammalian SCN to screen for novel, potentially conserved, molecules regulating sleep timing. From this screen, we identified Transducer of ERB-B2 (Tob), as a molecule required for proper sleep timing in *Drosophila*. Knockdown of *tob* causes an advance of sleep onset at night in constant darkness. Tob protein levels cycle under clock control, and Tob acts in a subset of clock neurons to regulate their synaptic strength and thereby sleep onset timing. Our data suggest that Tob is a novel clock output molecule that enhances postsynaptic potentiation in specific clock neurons to regulate the timing of sleep onset at night.

## Material and Methods

**Animals.** Flies were raised on standard food containing molasses, cornmeal, and yeast at 25°C. For all behavioral experiments, mated females were used, and flies were generated in the *iso31* background or backcrossed to the *iso31* background for at least four generations (Ryder et al., 2004).

**Genetic screen.** Candidate genes for the genetic screen were selected based on the following methods:

1. Enriched in the SCN: A list of genes differentially expressed in the SCN was obtained using Allen Brain Atlas in situ hybridization data in the mouse brain. A differential search was conducted comparing SCN (target) expression levels to those across the entire

cerebrum (contrast) using the built-in search tools. After identifying a list of all candidate genes with higher-than-average expression (fold change >1), each gene was manually rated based on SCN expression (YES/NO) and specificity of expression in SCN using a subjective scale (SCN only/strongly specific/moderately specific/mildly specific). Genes that were at least moderately specific were included.

2. Cycling in the SCN: A list of genes was collated from published datasets that performed RNA-seq of mouse SCN over a 24 h light/dark cycle and identified oscillatory genes (Panda et al., 2002; Pembroke et al., 2015; Bedont et al., 2017).

**Behavior.** Behavioral experiments were performed as previously described (Liu et al., 2014). For most experiments, 2–4-d-old mated females were loaded into wax- and yarn-sealed glass tubes with 5% sucrose in agar. For GeneSwitch experiments, 1–3-d-old females were kept on Kimwipes (Kimberly-Clark Worldwide) soaked with 1 ml of 5% sucrose solution containing 500 mM RU486 in 80% ethanol or 80% ethanol alone control for 24 h prior to loading. Flies in the experimental group were then loaded into 5% sucrose-agar glass tubes containing 200 mM RU486 dissolved in EtOH. Flies were allowed to recover from CO<sub>2</sub> anesthesia for ~36 h prior to data collection. Locomotion was measured using *Drosophila* Activity Monitoring System devices (DAMS, TriKinetics) at 23°C and 60% relative humidity. Sleep was identified as 5 min periods of consolidated immobility, as described previously (Shaw et al., 2000).

Sleep behavior was quantified using SleepLab (Joiner et al., 2006), a MATLAB-based (MathWorks) custom software. For analysis of LD sleep parameters, 2 d of LD were used; for analysis of DD sleep parameters, 3 d of DD were used. Sleep onset latency was generally calculated as the time of first sleep bout after ZT12 (Liu et al., 2014). However, in the GeneSwitch experiments, RU486 treatment alone affected the shape of the sleep profile. Thus, to address this confound, sleep latency in the GeneSwitch experiments was calculated as the first time after ZT12 where sleep amount is >10 min per 30 min bin for three consecutive bins. Mechanical sleep deprivation was performed using an analog VX-s-2500 Multitube Vortexer (VWR) with a Vortexer Mounting Plate (TriKinetics). Shaking was performed for 3 s every 1 min from ZT12–ZT24. Sleep rebound was calculated from ZT0–ZT6 on the following day, by comparing sleep amount during that time versus undisturbed controls.

Analysis of circadian parameters was performed on locomotor activity data from 7 d of DD using ClockLab (Actimetrics) software. Period length was calculated by chi-square periodogram analysis, using a confidence level of 0.01. Rhythm strength was calculated using fast Fourier transform (FFT) analysis. PHASE (Persons et al., 2022) was used to analyze evening peak phase, which was calculated using the average activity from the first three days in DD. Flies with no activity during any of the 3 d were excluded from the analysis. Peak time was visually inspected and manually corrected by a blinded observer.

**Molecular biology.** The *UAS-tob* miR line was generated as previously described (Chen et al., 2007). Two 22mers from exons 4 and 6 of the *tob* gene were used for creating the hairpin loops in the microRNA construct: ACG GAA AAC AAT GAA AAT CAT G and AGT AGT AGC CAT CCA ATT CAA C. The construct was synthesized (GeneArt, Thermo Fisher Scientific) and inserted into pUAST using NotI. Using this construct, transgenic flies were generated in the *iso31* background via P-element mediated random insertion (Rainbow Transgenic).

**Immunohistochemistry.** Whole brain immunostaining was performed as previously described (Liu et al., 2016). Brains from male or female flies were dissected in PBS, fixed in 4% PFA for 20 min, and washed five times in PBST (PBS + 0.5% Triton X-100). After blocking in 10% normal goat serum in PBST, the brains were incubated for ~48 h at 4°C with primary antibodies: mouse anti-PDF (C7, DSHB, 1:500), guinea pig anti-Tob (White-Grindley et al., 2014, 1:50), chicken anti-RFP (600-901-379, Rockland, 1:500), or rabbit anti-dsRed antibodies

(632496, Takara, 1:200). Brains were then washed for ~24 h and incubated with DAPI (10236276001, Millipore, 1:1,000) and secondary antibodies: Alexa 488 anti-guinea pig (A-11073, Invitrogen, 1:1,000), Alexa 647 anti-mouse (A-21235, Invitrogen, 1:1,000), Alexa 647 anti-chicken (A-21449, Invitrogen, 1:1,000), or Alexa 647 anti-rabbit (A27040, Invitrogen, 1:1,000) at 4°C for ~24 h. The brains were mounted in Vectashield (VectorLabs) for confocal imaging on an inverted LSM800 (Zeiss) with Airyscan detector, using ZEN 2.3 (Zeiss), C Plan-Apochromat 63×/1.4 oil objective (Zeiss). Each slice was 1,176 px × 1,176 px (33.8 mm × 33.8 mm) and 1.5 mm thick.

ImageJ was used to quantify total, cytoplasmic, and nuclear fluorescence signal intensity in immunohistochemistry data collected using confocal imaging. For each cell, the slice with the strongest DAPI signal was used. Two ROIs were drawn for analysis: around the entire cell (ROI<sub>1</sub>) and around the nuclear region marked by the DAPI signal (ROI<sub>2</sub>). Fluorescence signal intensity was quantified as the following:

$$\text{Total fluorescence intensity} = \text{Integrated Density}_{\text{ROI1}} / \text{Area}_{\text{ROI1}}$$

$$\begin{aligned} \text{Cytoplasmic fluorescence intensity} \\ = (\text{Integrated Density}_{\text{ROI1}} - \text{Integrated Density}_{\text{ROI2}}) / \\ (\text{Area}_{\text{ROI1}} - \text{Area}_{\text{ROI2}}) \end{aligned}$$

$$\begin{aligned} \text{Nuclear fluorescence intensity} \\ = \text{Integrated Density}_{\text{ROI2}} / \text{Area}_{\text{ROI2}} \end{aligned}$$

**Electrophysiology.** Flies were chilled on ice (up to 10 min) for anesthesia and placed in a dissecting chamber following isolation of the head. Brains were removed and dissected in a *Drosophila* physiological saline solution (in mM, 101 NaCl, 3 KCl, 1 CaCl<sub>2</sub>, 4 MgCl<sub>2</sub>, 1.25 NaH<sub>2</sub>PO<sub>4</sub>, 20.7 NaHCO<sub>3</sub>, and 5 glucose, with osmolarity adjusted to 238–245 mOsm and pH 7.2), which was prebubbled with 95% O<sub>2</sub> and 5% CO<sub>2</sub>. The glial sheath surrounding the brain was focally and carefully removed by using sharp forceps after treating with an enzymatic cocktail, collagenase (0.1 mg/ml), protease XIV (0.2 mg/ml), and dispase (0.3 mg/ml), at 22°C for 1 min to increase the likelihood of a successful recording. Using a small stream of saline, which was pressure ejected from a large-diameter pipette, the surface of the cell body was cleaned under a dissection microscope. LNd neurons were genetically labeled based on *Mai179-GAL4*, *pdf-GAL80>UAS-mCD8::GFP* and visualized via GFP fluorescence by using a PE300 CoolLED illumination system (CoolLED) on a fixed-stage upright microscope (BX51WI; Olympus). One neuron per brain was recorded. Sharp electrode intracellular recordings of LNds neurons were performed essentially as described (Nguyen et al., 2022) in order to clearly dissociate action potential spikes from postsynaptic potentials (PSPs). Sharp electrodes from quartz glass with a filament (OD/ID, 1.2/0.6 mm) were made with a laser-based micropipette puller (P-2000, Sutter Instrument) and backfilled with 1 mM KCl, with resistances of 120–190 MΩ. Solutions were filtered by using a syringe filter with a pore size of 0.02 μm (Anotop 10, Whatman). We inserted the electrode into the cell body of GFP-expressing LNd neurons, and impalements of the intracellular electrode were often facilitated using the shortest “buzz” pulses—only buzzing when the electrode was not moving. Recordings of membrane potentials commenced after the cell membrane potential was stable, as it usually took at least 1 min to stabilize the cell membrane potential. To reliably separate depolarizing PSPs, a tonic hyperpolarizing current was injected into the targeted cell to facilitate the measurement of PSPs. Somatic membrane potential level was kept between –105 and –110 mV. Recordings were acquired with an Axoclamp 2B with HS-2A ×1 LU headstage (Molecular Devices) and sampled with Digidata 1550B interface, which were controlled on a computer using pClamp 11 software. The signals were sampled at 10 kHz and low-pass filtered at 1 kHz.

Electrophysiological analysis was then performed in MATLAB (MathWorks). To detect and quantify spontaneous PSPs, a median filter with a time constant of 3 ms was applied to the unfiltered membrane potential. We also computed background noise power based on RMS values from all-points amplitude in each dataset and used them

to define both event finding and noise rejection criteria, which consisted of minimum allowed amplitude. All detected PSP events as well as their peak and quantified amplitudes were visualized to manually check computed results by visual inspection. After sorting individual PSP epochs, their amplitude was then defined as the difference between the maximum/minimum potential of each PSP and the mean membrane potential of the entire trace. Relative PSP rise time was calculated as interval between 20 and 80% of the peak amplitude relative to the baseline.

**Statistical analysis.** Statistical analyses were performed using Prism 9.4.0 (GraphPad). For comparisons between two non-normally distributed groups, Mann–Whitney tests were used. For comparisons between multiple groups, either one-way ANOVA with post hoc Tukey’s test or Kruskal–Wallis test with Dunn’s multiple-comparisons test were used, for normally distributed or non-normally distributed data, respectively.

## Results

### Identification of *tob* as a regulator of sleep onset timing

The *Drosophila* clock network shares important similarities with the mammalian SCN, both consisting of interconnected oscillators synchronized with neuropeptides and both directly regulating sleep (Dubowy and Sehgal, 2017; Collins et al., 2020; Shafer and Keene, 2021). Therefore, we conducted a large-scale genetic screen in *Drosophila* using candidates derived from mouse SCN to uncover potentially conserved molecular mechanisms for the circadian regulation of sleep (Fig. 1A). Using publicly available datasets (Panda et al., 2002; Pembroke et al., 2015; Bedont et al., 2017; Allen Mouse Brain Atlas), we identified 855 genes enriched and/or rhythmically expressed in the mouse SCN. From this list, 638 homologous genes were found in the *Drosophila* genome. We performed pan-neuronal RNAi knockdown of 611 of these homologous genes and assessed sleep phenotypes. From the primary screen, 45 genes were identified as putative sleep-regulating genes, among which 18 yielded reproducible data consistent with a role in modulating sleep. The phenotype observed with *tob* knockdown was one of the strongest identified in the screen. *Tob* knockdown significantly advanced the timing of sleep onset at night in constant darkness (DD; Fig. 1B).

*Tob* is part of the antiproliferative B-cell translocation gene (BTG) protein family, defined by the BTG protein domain that is highly conserved from worm to human (Fig. 1C), and has not previously been implicated in sleep or circadian rhythms. *Tob* regulates transcription and translation via its BTG and cytoplasmic polyadenylation element binding (CPEB)-interacting domains (Suzuki, 2002; Yoshida et al., 2003; Hosoda et al., 2011; Ogami et al., 2014) and contains putative nuclear localization signal (NLS) and nuclear export signal (NES) domains that facilitate its translocation between nucleus and cytoplasm (Kawamura-Tsuzuku et al., 2004).

We first reproduced the pan-neuronal *tob* knockdown phenotype using two independent RNAi lines (*UAS-tob RNAi #1* and *UAS-tob RNAi #2*) and a microRNA line (*UAS-tob miR*) that we generated. Pan-neuronal *tob* knockdown resulted in advanced sleep onset at night in DD using these three independent effector lines (Fig. 1D,E; Table 1). In contrast, pan-neuronal *tob* knockdown did not consistently alter total daily activity, daytime sleep amount, night-time sleep amount, sleep bout number, or sleep bout duration in 12 h light/dark (LD) or DD or sleep onset latency in LD (Table 2).

To confirm that the *UAS-tob RNAi #1*, *UAS-tob RNAi #2*, and *UAS-tob miR* lines could knockdown *Tob* expression, we drove expression of these transgenes using *pdf-GAL4* and quantified *Tob* levels in the large ventrolateral neurons (l-LNVs) following

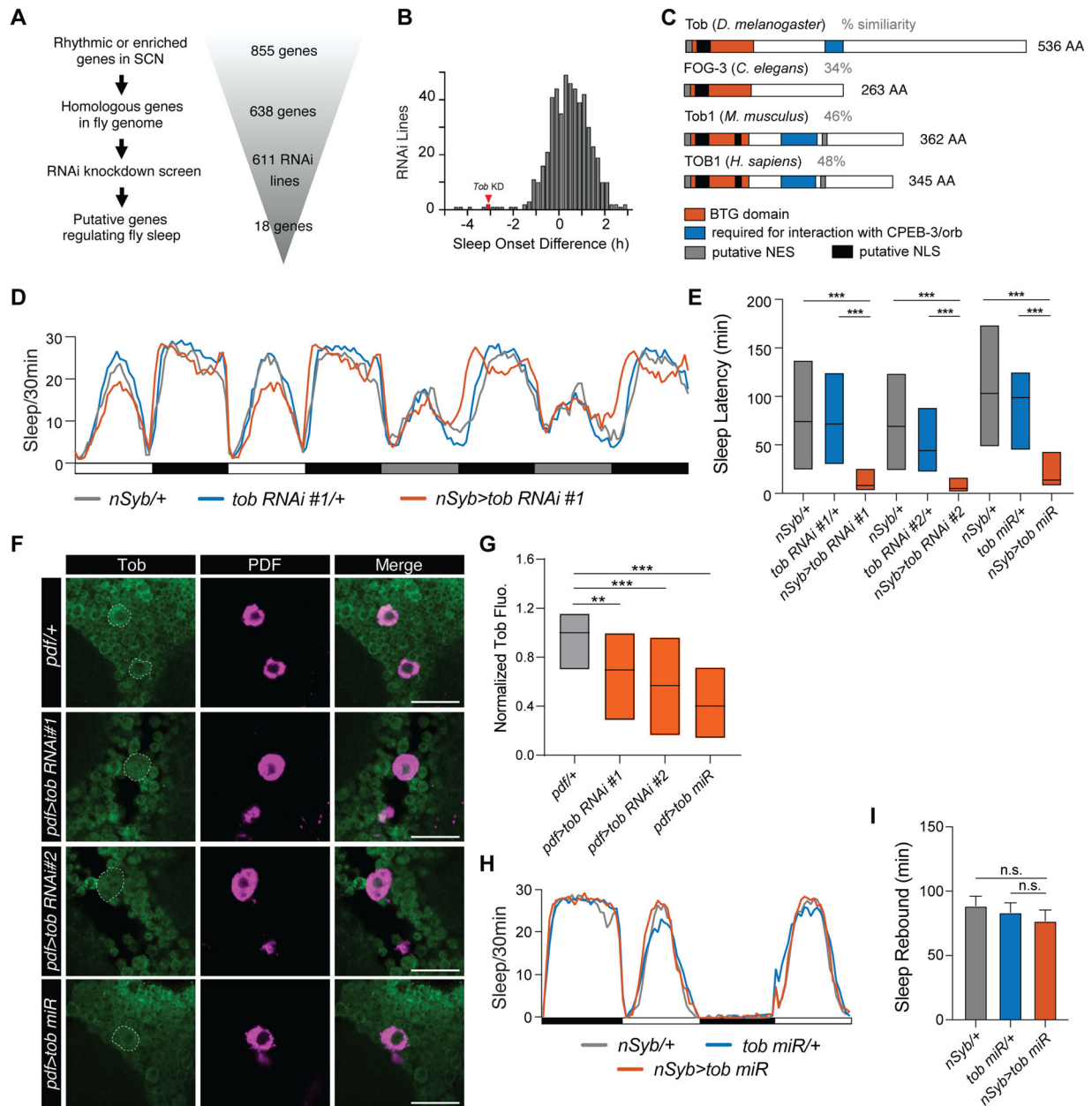


**Figure 1.** A genetic screen identifies Tob as a novel regulator of sleep onset timing at night. **A**, Schematic for the “SCN fly behavioral screen.” **B**, Histogram showing sleep onset difference of RNAi lines from the screen ( $n = 611$  RNAi lines). **C**, Schematic showing conserved domains in Tob across different species. **D**, Sleep profile of  $nSyb-GAL4>ctrl$  (gray),  $ctrl>UAS-tob$  RNAi #1 (blue), and  $nSyb-GAL4>UAS-tob$  RNAi #1 (red). White/black boxes denote LD, and gray/black boxes denote DD. **E**, Quantification shown as simplified box plots (25%, median, 75%) for sleep onset latency of  $nSyb-GAL4>ctrl$  (gray,  $n = 43$ ),  $ctrl>UAS-tob$  RNAi #1 (blue,  $n = 40$ ),  $nSyb-GAL4>UAS-tob$  RNAi #1 (red,  $n = 40$ ),  $nSyb-GAL4>ctrl$  (gray,  $n = 43$ ),  $ctrl>UAS-tob$  RNAi #2 (blue,  $n = 45$ ), and  $nSyb-GAL4>UAS-tob$  RNAi #2 (red,  $n = 31$ ),  $nSyb-GAL4>ctrl$  (gray,  $n = 43$ ),  $ctrl>UAS-tob$  miR (blue,  $n = 44$ ), and  $nSyb-GAL4>UAS-tob$  miR (red,  $n = 41$ ). **F**, Representative confocal images of I-LNv cell bodies (white dotted line) showing anti-Tob staining (green), anti-PDF staining (magenta), or merged channels in  $pdf-GAL4>ctrl$  ( $n = 17$ ),  $pdf-GAL4>UAS-tob$  RNAi #1 ( $n = 17$ ),  $pdf-GAL4>UAS-tob$  RNAi #2 ( $n = 16$ ), and  $pdf-GAL4>UAS-tob$  miR ( $n = 15$ ) flies at ZT12. Scale bar, 100  $\mu$ m. **G**, Simplified box plots showing normalized Tob signal for the animals in **F**. Anti-Tob fluorescence signal for experimental animals was normalized to the signal for  $pdf-GAL4>ctrl$  flies. **H**, Sleep profile of  $nSyb-GAL4>ctrl$  (gray),  $ctrl>UAS-tob$  miR (blue), and  $nSyb-GAL4>UAS-tob$  miR (red) flies with 12 h sleep deprivation (SD) from ZT12–ZT24. **I**, Quantification of sleep rebound over the 6 h period from ZT0 to ZT6 following SD for  $nSyb-GAL4>ctrl$  ( $n = 43$ , gray),  $ctrl>UAS-tob$  miR ( $n = 61$ , blue), and  $nSyb-GAL4>UAS-tob$  miR ( $n = 39$ , red) flies. \*, \*\*\*, and n.s. denote  $p < 0.05$ ,  $p < 0.001$ , and not significant, respectively.

Tob immunostaining using a previously described anti-Tob antibody (White-Grindley et al., 2014). These findings demonstrated that expression of all three transgenes significantly reduced Tob levels, with the greatest effect seen with the  $UAS-tob$  miR line (Fig. 1F,G; Table 1). To ensure that this sleep onset advance phenotype did not relate to an alteration in the homeostatic regulation of sleep, we also performed pan-neuronal knockdown of Tob and assessed sleep rebound following 12 h (ZT12–ZT24) mechanical sleep deprivation (SD). No difference in sleep

rebound was observed in  $nSyb-GAL4>UAS-tob$  miR flies, compared with GAL4 or UAS alone controls (Fig. 1H,I; Table 1).

To address whether the sleep onset advance observed with  $tob$  knockdown was due to developmental effects, we also performed temporally restricted  $tob$  knockdown using  $nSyb-GeneSwitch$  (Nicholson et al., 2008). A sleep onset advance phenotype was observed in DD when  $tob$  knockdown was induced by RU486 (Fig. 2A,B; Table 1). We next asked whether Tob overexpression would conversely produce a delay in sleep onset at night. To do

**Table 1. Details for statistical tests in Figures 1–6**

Figure	Comparisons	Statistical test	<i>p</i>	Test statistics	Replicates
1E	<i>nSyb-G4/+</i> and <i>nSyb-G4&gt;tob</i> RNAi #1	Kruskal–Wallis test, post hoc Dunn's	<0.0001	<i>H</i> = 124.3	3
	<i>tob</i> RNAi #1/+ and <i>nSyb-G4&gt;tob</i> RNAi #1	Kruskal–Wallis test, post hoc Dunn's	<0.0001		3
	<i>nSyb-G4/+</i> and <i>nSyb-G4&gt;tob</i> RNAi #2	Kruskal–Wallis test, post hoc Dunn's	<0.0001		3
	<i>tob</i> RNAi #2/+ and <i>nSyb-G4&gt;tob</i> RNAi #2	Kruskal–Wallis test, post hoc Dunn's	<0.0001		3
	<i>nSyb-G4/+</i> and <i>nSyb-G4&gt;tob</i> miR	Kruskal–Wallis test, post hoc Dunn's	<0.0001		3
1G	<i>tob</i> miR/+ and <i>nSyb-G4&gt;tob</i> miR	Kruskal–Wallis test, post hoc Dunn's	<0.0001		3
	<i>pdf-G4/+</i> and <i>pdf-G4&gt;tob</i> RNAi #1	Kruskal–Wallis test, post hoc Dunn's	0.0067	<i>H</i> = 19.82	3
	<i>pdf-G4/+</i> and <i>pdf-G4&gt;tob</i> RNAi #2	Kruskal–Wallis test, post hoc Dunn's	<0.0001		3
1I	<i>pdf-G4/+</i> and <i>pdf-G4&gt;tob</i> miR	Kruskal–Wallis test, post hoc Dunn's	<0.0001		3
	<i>nSyb-G4/+</i> and <i>nSyb-G4&gt;tob</i> miR	One-way ANOVA, post hoc Tukey	0.5865	$F_{(2,140)} = 0.488$	3
2B	<i>tob</i> miR/+ and <i>nSyb-G4&gt;tob</i> miR	One-way ANOVA, post hoc Tukey	0.8209		3
	<i>nSybGS&gt;tob</i> miR +RU486 and <i>nSybGS/+</i> +RU486	Kruskal–Wallis test, post hoc Dunn's	<0.0001	<i>H</i> = 39.98	2
2D	<i>nSybGS&gt;tob</i> miR +RU486 and <i>nSybGS&gt;tob</i> miR -RU486	Kruskal–Wallis test, post hoc Dunn's	0.0008		2
	<i>nSyb-G4/+</i> and <i>nSyb-G4&gt;tob</i>	Kruskal–Wallis test, post hoc Dunn's	0.0268	<i>H</i> = 10.86	3
3D	<i>Tob/+</i> and <i>nSyb-G4&gt;Tob</i>	Kruskal–Wallis test, post hoc Dunn's	0.0062		3
	ZT0 and ZT6	Kruskal–Wallis test, post hoc Dunn's	0.0011	<i>H</i> = 21.98	3
	ZT0 and ZT12	Kruskal–Wallis test, post hoc Dunn's	0.0023		3
3E	ZT0 and ZT18	Kruskal–Wallis test, post hoc Dunn's	>0.9999		3
	ZT0 and ZT6	Kruskal–Wallis test, post hoc Dunn's	0.0005	<i>H</i> = 25.03	3
	ZT0 and ZT12	Kruskal–Wallis test, post hoc Dunn's	0.0012		3
3F	ZT0 and ZT18	Kruskal–Wallis test, post hoc Dunn's	>0.9999		3
	ZT0 and ZT6	Kruskal–Wallis test, post hoc Dunn's	0.1082	<i>H</i> = 7.063	3
	ZT0 and ZT12	Kruskal–Wallis test, post hoc Dunn's	0.3097		3
3J	ZT0 and ZT18	Kruskal–Wallis test, post hoc Dunn's	>0.9999		3
	CT0 and CT12	Mann–Whitney test	<0.0001	<i>U</i> = 1,282.00	3
	CT0 and CT12	Mann–Whitney test	<0.0001	<i>U</i> = 1,259.00	3
3K	CT0 and CT12	Mann–Whitney test	0.0024	<i>U</i> = 1,465.00	3
3P	ZT0 and ZT12	Mann–Whitney test	0.200	<i>U</i> = 631.00	2
3Q	ZT0 and ZT12	Mann–Whitney test	0.158	<i>U</i> = 618.00	2
3R	ZT0 and ZT12	Mann–Whitney test	0.933	<i>U</i> = 751.00	2
4B	<i>mai179-G4, pdf-G80&gt;tob</i> RNAi#1 and <i>tob</i> RNAi#1/+	Kruskal–Wallis test, post hoc Dunn's	0.0017	<i>H</i> = 14.62	3
	<i>pdf-G4&gt;tob</i> RNAi #1 and <i>tob</i> RNAi#1/+	Kruskal–Wallis test, post hoc Dunn's	>0.9999		2
	<i>R51H05-G4&gt;tob</i> RNAi #1 and <i>tob</i> RNAi#1/+	Kruskal–Wallis test, post hoc Dunn's	>0.9999		2
	<i>R1B03-AD;R65D05-DBD&gt;tob</i> RNAi #1 and <i>tob</i> RNAi#1/+	Kruskal–Wallis test, post hoc Dunn's	>0.9999		2
	<i>mai179-G4, pdf-G80&gt;tob</i> miR and <i>mai179-G4, pdf-G80/+</i>	Kruskal–Wallis test, post hoc Dunn's	0.0001	<i>H</i> = 20.26	3
4D	<i>mai179-G4, pdf-G80&gt;tob</i> miR and <i>tob</i> miR/+	Kruskal–Wallis test, post hoc Dunn's	0.0004		3
	<i>MB122B&gt;tob</i> miR and <i>MB122B/+</i>	Kruskal–Wallis test, post hoc Dunn's	<0.0001	<i>H</i> = 27.25	3
4F	<i>MB122B&gt;tob</i> miR and <i>tob</i> miR/+	Kruskal–Wallis test, post hoc Dunn's	0.0033		3
	<i>mai179-G4, pdf-G80&gt;Tob</i> and <i>mai179-G4, pdf-G80/+</i>	Kruskal–Wallis test, post hoc Dunn's	0.0005	<i>H</i> = 17.58	3
5D	<i>mai179-G4, pdf-G80&gt;Tob</i> and <i>UAS-tob/+</i>	Kruskal–Wallis test, post hoc Dunn's	0.0006		3
	ZT0 and ZT6	Kruskal–Wallis test, post hoc Dunn's	0.0012	<i>H</i> = 34.97	3
	ZT0 and ZT12	Kruskal–Wallis test, post hoc Dunn's	>0.9999		3
5E	ZT0 and ZT18	Kruskal–Wallis test, post hoc Dunn's	0.5850		3
	ZT0 and ZT6	Kruskal–Wallis test, post hoc Dunn's	0.0011	<i>H</i> = 34.45	3
	ZT0 and ZT12	Kruskal–Wallis test, post hoc Dunn's	>0.9999		3
5F	ZT0 and ZT18	Kruskal–Wallis test, post hoc Dunn's	0.6801		3
	ZT0 and ZT6	Kruskal–Wallis test, post hoc Dunn's	0.0142	<i>H</i> = 40.30	3
	ZT0 and ZT12	Kruskal–Wallis test, post hoc Dunn's	>0.9999		3
5J	ZT0 and ZT18	Kruskal–Wallis test, post hoc Dunn's	0.0405		3
	CT6 and CT18	Mann–Whitney test	<0.0001	<i>U</i> = 58.00	3
	CT6 and CT18	Mann–Whitney test	0.0003	<i>U</i> = 104.00	3
5L	CT6 and CT18	Mann–Whitney test	0.0006	<i>U</i> = 113.00	3
5P	ZT6 and ZT18	Mann–Whitney test	0.5394	<i>U</i> = 186.00	3
5Q	ZT6 and ZT18	Mann–Whitney test	0.4732	<i>U</i> = 182.00	3
5R	ZT6 and ZT18	Mann–Whitney test	0.6891	<i>U</i> = 194.00	3
6B	<i>mai179-G4, pdf-G80&gt;ORK1DC1</i> and <i>mai179-G4, pdf-G80&gt;ORK1DNC</i>	Kruskal–Wallis test, post hoc Dunn's	0.0019	<i>H</i> = 11.95	2
	<i>mai179-G4, pdf-G80&gt;UAS-ORK1DC1</i> and <i>UAS-ORK1DC1/+</i>	Kruskal–Wallis test, post hoc Dunn's	0.0248		2
	<i>mai179-G4, pdf-G80&gt;UAS-ORK1DC1</i> and <i>mai179-G4, pdf-G80/+</i>	Kruskal–Wallis test, post hoc Dunn's	0.0320		2
6D	PSP amplitude: control ZT0 vs ZT12	One-way ANOVA, post hoc Tukey	<0.0001	$F_{(3,18)} = 25.20$	
	PSP amplitude: <i>Tob</i> KD ZT0 vs ZT12	One-way ANOVA, post hoc Tukey	0.0076		
	PSP amplitude: ZT12 control vs <i>Tob</i> KD	One-way ANOVA, post hoc Tukey	0.0037		
	PSP amplitude: ZT0 control vs <i>Tob</i> KD	One-way ANOVA, post hoc Tukey	0.9636		
6E	PSP frequency: control ZT0 vs ZT12	One-way ANOVA, post hoc Tukey	0.9357	$F_{(3,18)} = 2.577$	
	PSP frequency: <i>Tob</i> KD ZT0 vs ZT12	One-way ANOVA, post hoc Tukey	0.0685		
	PSP frequency: ZT12 control vs <i>Tob</i> KD	One-way ANOVA, post hoc Tukey	0.5240		

(Table continues.)

Table 1. Continued

Figure	Comparisons	Statistical test	<i>p</i>	Test statistics	Replicates
6F	PSP frequency: ZT0 control vs Tob KD	One-way ANOVA, post hoc Tukey	0.8841	$F_{(3,18)} = 82.56$	
	PSP rise time: control ZT0 vs ZT12	One-way ANOVA, post hoc Tukey	<0.0001		
	PSP rise time: Tob KD ZT0 vs ZT12	One-way ANOVA, post hoc Tukey	<0.0001		
	PSP rise time: ZT12 control vs Tob KD	One-way ANOVA, post hoc Tukey	0.0025		
	PSP rise time: ZT0 control vs Tob KD	One-way ANOVA, post hoc Tukey	0.9915		

this, we used a pan-neuronal driver in combination with a *UAS-tob-tdTomato* transgene (White-Grindley et al., 2014) and assayed sleep phenotypes. As predicted, broad neuronal overexpression of Tob resulted in a significant sleep onset delay in DD, compared with controls (Fig. 2C,D; Table 1). Tob overexpression did not consistently alter daily activity in LD or DD, sleep latency in LD, or daytime sleep amount in LD (Table 3). Daytime sleep amount was reduced in DD, and night-time sleep amount was reduced in LD and DD. Sleep bout consolidation was decreased in LD, while more, but shorter, sleep bouts were seen in DD (Table 3). Taken together, these data suggest that Tob acts in neurons to regulate the timing of sleep onset at night in *Drosophila*.

### Tob levels cycle under clock control

Because Tob regulates the timing of sleep, a rhythmic behavior, we hypothesized that Tob is a clock output molecule that cycles under clock control. Single-cell RNA sequencing data has shown that Tob is expressed in the clock network, including the l-LNVs (Ma et al., 2021); thus, we first focused our analysis on these PDF<sup>+</sup> (Pigment-Dispersing Factor) l-LNVs, which have large cell bodies allowing for convenient analysis of subcellular protein localization. We performed Tob immunostaining and assessed Tob levels in l-LNVs. In wild-type flies across four timepoints under LD conditions, Tob levels exhibit a diurnal rhythm, peaking at ZT12 (Fig. 3A–D; Table 1). Although Tob was found in both cytoplasmic and nuclear compartments, Tob cycling was mainly driven by changes of Tob level in the cytoplasm (Fig. 3E,F; Table 1). Previously, *tob* mRNA has been shown to cycle in the mouse SCN, peaking at ZT6 (Pembroke et al., 2015).

To address whether this cycling is circadian in nature, we repeated these experiments in DD and found that Tob cycling persisted in PDF<sup>+</sup> neurons l-LNVs (Fig. 3G–L; Table 1). Moreover, rhythmic expression of Tob was lost in *per*<sup>01</sup> mutant flies in LD, with similar levels at ZT0 and ZT12 (Fig. 3M–R; Table 1). Taken together, these data indicate that Tob expression is under clock control, suggesting that Tob is a clock output molecule that regulates the timing of sleep onset at night.

### Tob cycles in evening cells to regulate the timing of sleep onset at night

In *Drosophila*, distinct clock neurons are thought to shape different aspects of activity and sleep (Dubowy and Sehgal, 2017; Shafer and Keene, 2021). Given this knowledge and because Tob was identified from a screen of SCN genes, we hypothesized that Tob acts in a subset of clock neurons to modulate sleep timing. A previously published single-cell RNA-seq dataset found that *tob* mRNA is present in multiple subpopulations of *Drosophila* clock neurons including DN1a, LNd, fifth s-LNV, l-LNV, s-LNV, and DN1p and, among these, is especially enriched in DN1a, LNd, and l-LNV clusters (Fig. 4A; Ma et al., 2021).

Thus, we investigated whether knocking down *tob* in any of these subpopulations recapitulated the sleep onset advance phenotype with pan-neuronal *tob* knockdown. We found that *tob*

knockdown in l-LNV + s-LNV (using *pdf-GAL4*), DN1p (using *R51H11-GAL4*), or LPN (using *R11B03-AD*, *R65D05-DBD*) clusters had no effect on sleep onset timing. In contrast, *tob* knockdown in LNd + fifth s-LNV neurons (“evening neurons”) using *Mai179-GAL4*, *pdf-GAL80* resulted in an advanced sleep onset at night (Fig. 4B; Table 1). To further demonstrate that this phenotype localized to the evening neurons, we reproduced this finding using the *UAS-tob miR* transgene with *Mai179-GAL4*, *pdf-GAL80*, as well as *MB122B-split-GAL4* (Fig. 4C,D; Table 1). Knockdown of Tob in evening cells did not consistently alter daily activity in LD and DD, sleep latency in LD, daytime sleep amount in LD and DD, night-time sleep amount in LD and DD, or sleep consolidation in LD and DD (Table 4). We next assessed the effects of overexpressing Tob in LNd + fifth s-LNV neurons and found this manipulation delayed sleep onset at night (Fig. 4E,F; Table 1). Tob overexpression in evening cells did not consistently affect daily activity, sleep latency, or daytime or night-time sleep amount in LD, or sleep consolidation in LD or DD. However, in DD, daily activity was increased, while daytime and night-time sleep amount was decreased (Table 4).

We previously found that Tob levels cycle in the l-LNVs, and so we next asked whether Tob also cycles in the evening cells. Immunostaining for Tob in LNd + fifth s-LNV neurons across four timepoints revealed that Tob expression cycles in evening neurons, peaking at ZT6 and reaching a nadir at ZT18 (Fig. 5A–D; Table 1). In these cells, Tob cycling was observed in both cytoplasmic and nuclear compartments (Fig. 5E,F; Table 1). To demonstrate that this cycling was circadian in nature, we next examined Tob cycling in LNd neurons under DD conditions and the *per*<sup>01</sup> mutant background. These findings showed that Tob cycling persisted in these cells in constant darkness (Fig. 5G–L; Table 1) but was lost in the *per*<sup>01</sup> mutant background under LD conditions (Fig. 5M–R; Table 1). Together, these data suggest that Tob cycles in evening cells and is required in these cells to regulate the timing of sleep onset at night.

Because Tob acts in specific clock neurons to affect the timing of sleep onset at night, we asked whether this phenotype could be attributable to changes in circadian parameters. We first examined whether Tob knockdown or overexpression either pan-neuronally or in evening cells affected circadian period or rhythm strength using locomotor data from 7 d in DD. Neither circadian period length nor rhythm strength was consistently altered with these manipulations (Table 5). Another possibility is that the effect of Tob manipulations on sleep onset at night simply reflects an alteration in the phase of the evening activity peak. To address this possibility, we quantified the phase of the evening activity peak (Persons et al., 2022). We did not find consistent effects of either Tob knockdown or Tob overexpression using either pan-neuronal or an evening cell driver on the phase of the evening peak (Table 5). These data suggest that core clock function is largely intact in flies with Tob knockdown or overexpression and suggest that the sleep onset timing

Table 2. Additional sleep parameters related to Figure 1

Genotype	LD activity		LD sleep latency (min)		LD day sleep (min)		LD night sleep (min)		LD sleep bout number		LD sleep bout duration (min)	
	Mean ± SEM		Median (25–75%)		Mean ± SEM		Mean ± SEM		Mean ± SEM		Median (25–75%)	
<i>nSyb-G4&gt;UAS-tob RNAi #1</i>	1,239 ± 46.22		12 (8.37–18.25)		275.3 ± 10.72		562.4 ± 11.71		12.92 ± 0.58		44.93 (38.48–56.23)	
	$F_{(2,122)} = 0.021$		$H = 36.30$		$F_{(2,122)} = 1.87$		$F_{(2,122)} = 3.831$		$F_{(2,122)} = 0.6615$		$H = 0.4887$	
	vs G4: $p = 0.9875$		vs UAS: $p < 0.0001$		vs UAS: $p = 0.1413$		vs UAS: $p = 0.721$		vs UAS: $p = 0.4915$		vs UAS: $p > 0.9999$	
	vs G4: $p = 0.9988$		vs G4: $p < 0.0001$		vs G4: $p = 0.7877$		vs G4: $p = 0.0220$		vs G4: $p = 0.7643$		vs G4: $p > 0.9999$	
<i>UAS-tob RNAi #1/+</i>	1,228 ± 53.09		43.5 (23.25–65.75)		308.6 ± 14.03		548.4 ± 10.46		14.36 ± 1.02		43.40 (29.85–58.70)	
	1,242 ± 57.55		43.25 (12.0–90.38)		286.8 ± 12.10		513.8 ± 15.57		13.8 ± 0.99		47.50 (29.04–70.33)	
	870.3 ± 34.1		15.5 (7.5–22.25)		276.2 ± 16.56		663.8 ± 8.269		7.252 ± 0.7485		126.7 (84.68–224)	
	$F_{(2,114)} = 18.75$		$H = 32.44$		$F_{(2,114)} = 4.492$		$F_{(2,114)} = 39.92$		$F_{(2,114)} = 28.28$		$H = 45.92$	
<i>nSyb-G4&gt;UAS-tob RNAi #2</i>	vs UAS: $p = 0.0599$		vs UAS: $p < 0.0001$		vs UAS: $p = 0.0878$		vs UAS: $p < 0.0001$		vs UAS: $p < 0.0001$		vs UAS: $p < 0.0001$	
	vs G4: $p < 0.0001$		vs G4: $p = 0.0053$		vs G4: $p = 0.0102$		vs G4: $p < 0.0001$		vs G4: $p < 0.0001$		vs G4: $p < 0.0001$	
	1,015 ± 40.22		31.75 (2.63–47.50)		233 ± 12.28		570.6 ± 9.883		13.85 ± 0.67		44.5 (31.11–65.84)	
	1,242 ± 45.17		20.5 (15.75–33.00)		216.1 ± 12.8		531.2 ± 10.42		14.89 ± 0.72		36.10 (27.44–58.89)	
<i>nSyb-G4/+</i>	1,169 ± 45.98		14 (11–19.5)		209.1 ± 11.02		647.1 ± 8.062		7.20 ± 0.64		114 (69.83–222)	
	$F_{(2,130)} = 5.797$		$H = 21.38$		$F_{(2,128)} = 6.090$		$F_{(2,128)} = 17.51$		$F_{(2,128)} = 17.83$		$H = 35.15$	
	vs UAS: $p = 0.0090$		vs UAS: $p < 0.0001$		vs UAS: $p = 0.0019$		vs UAS: $p = 0.0064$		vs UAS: $p < 0.0001$		vs UAS: $p = 0.0032$	
	vs G4: $p = 0.9868$		vs G4: $p = 0.1366$		vs G4: $p = 0.2229$		vs G4: $p < 0.0001$		vs G4: $p < 0.0001$		vs G4: $p < 0.0001$	
<i>UAS-tob miR/+</i>	1,293 ± 46.31		27 (16.5–44.25)		280.8 ± 12.09		600.6 ± 9.248		11.45 ± 0.78		63.65 (38.83–107.3)	
	1,140 ± 61.03		17 (14.25–22.0)		243.5 ± 18.91		558.2 ± 13.40		13.07 ± 0.69		46.58 (33.51–65.03)	
	DD activity		DD Day sleep (min)		DD Night sleep (min)		DD Sleep bout number		DD Sleep bout duration (min)			
	Mean ± SEM		Mean ± SEM		Mean ± SEM		Mean ± SEM		Mean ± SEM			
<i>nSyb-G4&gt;UAS-tob RNAi #1</i>	1,222 ± 52.10		311.5 ± 17.08		505.2 ± 14.86		18.37 ± 0.62		18.15 (15.24–21.87)			
	$F_{(2,120)} = 1.112$		$F_{(2,120)} = 3.283$		$F_{(2,120)} = 3.909$		$F_{(2,120)} = 2.867$		$H = 7.414$			
	vs UAS: $p = 0.2988$		vs UAS: $p = 0.0331$		vs UAS: $p = 0.5030$		vs UAS: $p = 0.0631$		vs UAS: $p = 0.0504$			
	vs G4: $p = 0.7332$		vs G4: $p = 0.2486$		vs G4: $p = 0.0175$		vs G4: $p = 0.1744$		vs G4: $p = 0.0582$			
<i>UAS-tob RNAi #1/+</i>	1,370 ± 74.97		248.6 ± 16.58		480.9 ± 12.99		15.66 ± 0.8		15.67 (11.61–19.50)			
	1,295 ± 76.22		272.5 ± 18.11		446.2 ± 16.90		16.27 ± 1.001		15.70 (10.67–20.07)			
	934 ± 88.83		373.2 ± 26.40		606.7 ± 15.49		10.74 ± 0.94		75.60 (51.43–163.2)			
	$F_{(2,116)} = 4.042$		$F_{(2,116)} = 14.15$		$F_{(2,116)} = 18.38$		$F_{(2,116)} = 12.29$		$H = 33.54$			
<i>nSyb-G4/+</i>	vs UAS: $p = 0.0878$		vs UAS: $p = 0.0008$		vs UAS: $p = 0.0015$		vs UAS: $p = 0.1253$		vs UAS: $p = 0.0029$			
	vs G4: $p = 0.0176$		vs G4: $p < 0.0001$		vs G4: $p < 0.0001$		vs G4: $p < 0.0001$		vs G4: $p < 0.0001$			
	1,150 ± 60.51		270.8 ± 14.36		530.1 ± 12.45		12.99 ± 0.6240		44.43 (33.10–64.18)			
	1,218 ± 63.07		228.9 ± 16.97		475.7 ± 15.70		16.34 ± 0.82		30.67 (22.77–48.27)			
<i>nSyb-G4&gt;UAS-tob RNAi #2</i>	1,334 ± 82.62		202 ± 16.29		552.1 ± 16.60		14.94 ± 0.85		40.87 (31.48–65.43)			
	$F_{(2,125)} = 10.89$		$F_{(2,125)} = 0.2927$		$F_{(2,125)} = 20.52$		$F_{(2,125)} = 1.976$		$H = 19.39$			
	vs UAS: $p = 0.0001$		vs UAS: $p = 0.9103$		vs UAS: $p = 0.0005$		vs UAS: $p = 0.5381$		vs UAS: $p > 0.9999$			
	vs G4: $p = 0.8130$		vs G4: $p = 0.7253$		vs G4: $p < 0.0001$		vs G4: $p = 0.6464$		vs G4: $p = 0.0002$			
<i>UAS-tob miR/+</i>	1,572 ± 78.63		201.2 ± 12.10		476.6 ± 12.69		14.91 ± 0.80		33.17 (25.53–60.27)			
	1,650 ± 87.51		176.1 ± 18.74		409.4 ± 18.62		14.76 ± 0.63		28.33 (19.73–42.17)			

These data are derived from the dataset shown in Figure 1C. One-way ANOVA with post hoc Tukey used for all variables, except for LD sleep latency, LD sleep bout duration, and DD sleep bout duration for which Kruskal–Wallis with post hoc Dunn's was used.

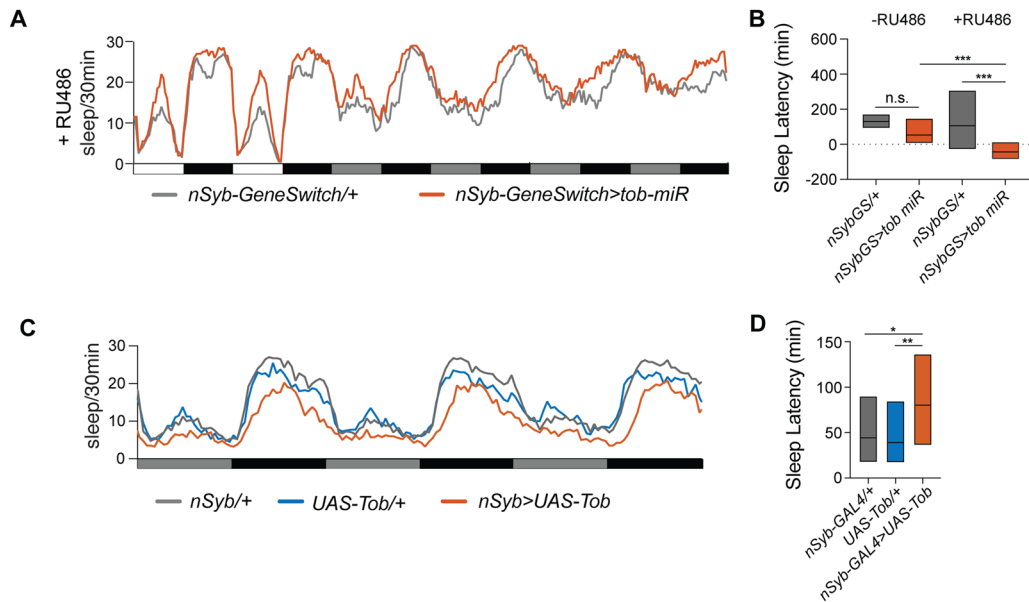


**Figure 2.** Conditional Tob knockdown advances and Tob overexpression delays sleep onset at night. **A**, Sleep profile with RU486 drug induction: *nSyb-GeneSwitch>ctrl* (gray), *nSyb-GeneSwitch>UAS-tob miR* (red). **B**, Simplified box plots for sleep onset latency in DD of *nSyb-GeneSwitch>ctrl* (gray,  $n = 41$ ) and *nSyb-GeneSwitch>UAS-tob miR* (red,  $n = 39$ ) without RU486 (-RU486); *nSyb-GeneSwitch>ctrl* (gray,  $n = 40$ ) and *nSyb-GeneSwitch>UAS-tob miR* (red,  $n = 41$ ) with RU486 drug induction (+RU486). **C**, Sleep profiles of *nSyb-GAL4>ctrl* (gray), *ctrl>UAS-tob-tdTomato* (blue), and *nSyb-GAL4>UAS-tob-tdTomato* (red). **D**, Simplified box plots for sleep onset latency in DD of *nSyb-GAL4>ctrl* (gray,  $n = 69$ ), *ctrl>UAS-tob-tdTomato* (blue,  $n = 56$ ), and *nSyb-GAL4>UAS-tob-tdTomato* (red,  $n = 56$ ). \*, \*\*, \*\*\*, and n.s. denote  $p < 0.05$ ,  $p < 0.01$ ,  $p < 0.001$ , and not significant, respectively.

**Table 3. Additional sleep parameters related to Figure 2**

Genotype	LD activity	LD sleep latency (min)	LD day sleep (min)	LD night sleep (min)	LD sleep bout number	LD sleep bout duration (min)
	Mean $\pm$ SEM	Median (25–75%)	Mean $\pm$ SEM	Mean $\pm$ SEM	Mean $\pm$ SEM	Median (25–75%)
<i>nSyb-G4&gt;UAS-tob</i>	1,534 $\pm$ 48.38 $F_{(2,165)} = 21.81$ vs UAS: $p = 0.9694$ vs G4: $p < 0.0001$	20.75 (13.13–37.25) $H = 7.46$ vs UAS: $p = 0.2421$ vs G4: $p > 0.9999$	160.9 $\pm$ 11.44 $F_{(2,165)} = 3.439$ vs UAS: $p = 0.0824$ vs G4: $p = 0.0491$	380.2 $\pm$ 13.86 $F_{(2,165)} = 51.63$ vs UAS: $p < 0.0001$ vs G4: $p < 0.0001$	17.37 $\pm$ 0.53 $F_{(2,165)} = 6.476$ vs UAS: $p = 0.0023$ vs G4: $p = 0.0220$	21.98 (16.86–28.41) $H = 48.36$ vs UAS: $p < 0.0001$ vs G4: $p < 0.0001$
<i>nSyb-G4</i>	1,161 $\pm$ 34.77	17.00 (11.50–33.75)	197.1 $\pm$ 9.48	546.5 $\pm$ 9.721	15.15 $\pm$ 0.60	38.98 (30.58–61.05)
<i>UAS-tob/+</i>	1,519 $\pm$ 50.80	32.50 (17.75–51.13)	193.7 $\pm$ 11.28	483.9 $\pm$ 11.1	14.53 $\pm$ 0.62	35.60 (26.54–50.68)
Genotype	DD activity	DD day sleep (min)	DD night sleep (min)	DD sleep bout number	DD sleep bout duration (min)	
	Mean $\pm$ SEM	Mean $\pm$ SEM	Mean $\pm$ SEM	Mean $\pm$ SEM	Median (25–75%)	
<i>nSyb-G4&gt;UAS-tob</i>	1,334 $\pm$ 51.58 $F_{(2,163)} = 10.60$ vs UAS: $p = 0.5194$ vs G4: $p = 0.0029$	146.6 $\pm$ 14.23 $F_{(2,163)} = 11.13$ vs UAS: $p < 0.0001$ vs G4: $p = 0.0014$	316.2 $\pm$ 12.95 $F_{(2,163)} = 58.66$ vs UAS: $p < 0.0001$ vs G4: $p < 0.0001$	22.44 $\pm$ 0.84 $F_{(2,163)} = 15.22$ vs UAS: $p = 0.0006$ vs G4: $p < 0.0001$	21.83 (17.67–28.03) $H = 67.48$ vs UAS: $p < 0.0001$ vs G4: $p < 0.0001$	
<i>nSyb-G4</i>	1,100 $\pm$ 41.61	213.2 $\pm$ 12.89	495.8 $\pm$ 10.39	16.78 $\pm$ 0.73	16.48 (13.93–20.73)	
<i>UAS-tob/+</i>	1,409 $\pm$ 52.60	228.8 $\pm$ 12.21	437.4 $\pm$ 12.39	18.45 $\pm$ 0.66	18.17 (15.27–21.32)	

These data are derived from the dataset shown in Figure 2D.

One-way ANOVA with post hoc Tukey used for all variables, except for LD sleep latency, LD sleep bout duration, and DD sleep bout duration for which Kruskal–Wallis with post hoc Dunn's was used.

effects seen with manipulation of Tob are not solely due to changes in circadian-related parameters.

### Tob enhances postsynaptic potentiation in evening cells

What is the impact of Tob knockdown on evening cell activity? It was previously shown that inhibiting the output of evening cells using tetanus toxin (TNT; Keller et al., 2002) results in earlier offset of evening activity (Guo et al., 2014). Thus, we asked if Tob knockdown advances sleep onset timing by reducing the excitability of evening cells. To decrease excitability of evening cells, we expressed dORK1, an open rectifier  $K^+$  channel, in these cells using *Mai179-GAL4*, *pdf-GAL80*. Compared with controls, *Mai179-GAL4*, *pdf-GAL80>UAS-dORK1DC1* flies exhibited an

advanced sleep onset at night in DD, similar to that seen with *tob* knockdown (Fig. 6A,B; Table 1). We next investigated the physiological consequences of manipulating Tob in evening cells by performing electrophysiological recordings in these cells, with or without *tob* knockdown at ZT0 and ZT12 (Fig. 6C–F). As has been previously described (Tang et al., 2022), we noted that the LNd neurons exhibited slow membrane potential oscillations in our ex vivo preparation that made the measurement of action potentials unreliable. Thus, we chose to perform sharp electrode intracellular recordings, rather than perforated patch-clamp recordings, to achieve stable current injection in current-clamp configuration. We restricted our analysis of LNd physiological properties to PSPs, a measure of synaptic strength. In wild-type



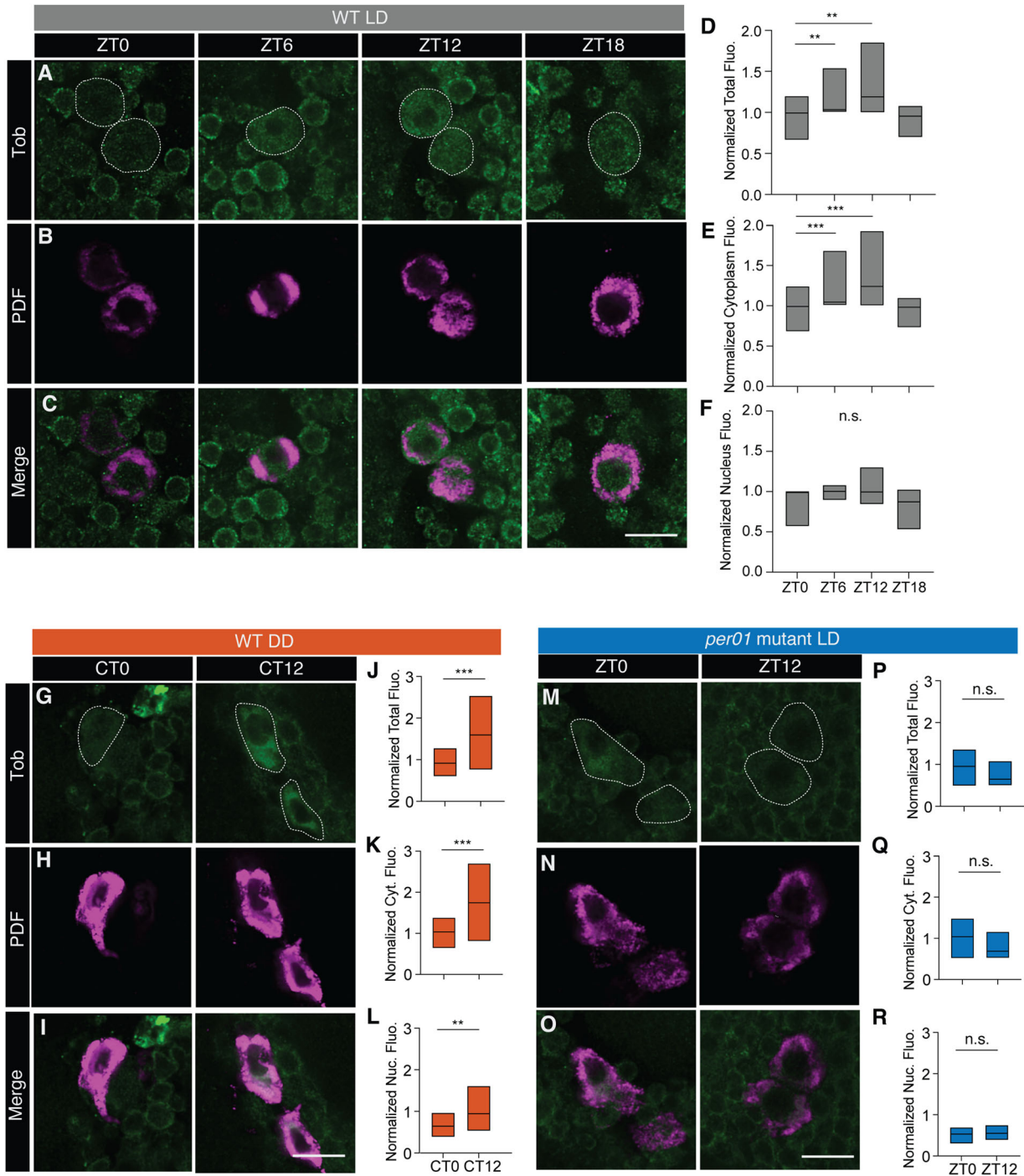


**Figure 3.** Tob levels cycle under clock control in l-LNvs. **A–F**, Whole-mount brain immunostaining of wild-type *iso31* flies at ZT0 ( $n = 11$ ), ZT6 ( $n = 14$ ), ZT12 ( $n = 11$ ), and ZT18 ( $n = 9$ ). **G–L**, Whole-mount brain immunostaining of wild-type *iso31* flies in DD at CT0 ( $n = 17$ ) and CT12 ( $n = 15$ ). **M–R**, Whole-mount brain immunostaining of *per01* mutant flies in LD at ZT0 ( $n = 8$ ) and ZT12 ( $n = 10$ ). Representative images, showing anti-Tob staining (**A,G,M**, green) in PDF<sup>+</sup> neuron cell bodies (white dotted line); anti-PDF staining (**B,H,N**, magenta); and merged signals (**C,I,O**). Simplified box plots showing normalized Tob signal in the cell body (**D,J,P**), cytoplasm (**E,K,Q**), and nucleus (**F,L,R**) of PDF<sup>+</sup> neurons. Scale bars, 10  $\mu$ m. \*\*, \*\*\*, and n.s. denote  $p < 0.01$ ,  $p < 0.001$ , and not significant, respectively.

animals, we observed cycling of PSP amplitude, with increased PSP amplitude at ZT12, compared with that at ZT0. Knockdown of Tob did not affect PSP amplitude at ZT0 but significantly reduced it at ZT12 (Fig. 6C,D; Table 1). PSP rise time also cycled in LN<sub>d</sub> neurons, with a steeper slope at ZT12 versus ZT0. Similarly, Tob knockdown did not affect PSP rise time at ZT0 but increased PSP rise time at ZT12 (Fig. 6F), suggesting increased synaptic distance and/or changes in postsynaptic

channel composition or function. In contrast, PSP frequency was not significantly altered between ZT0 and ZT12 in wild-type animals, nor with knockdown of Tob (Fig. 6E), suggesting the number of synapses and release probability were not affected by *tob* knockdown. Taken together, our data suggest that Tob promotes postsynaptic potentiation in evening cells at night, thereby maintaining evening activity and delaying sleep onset.

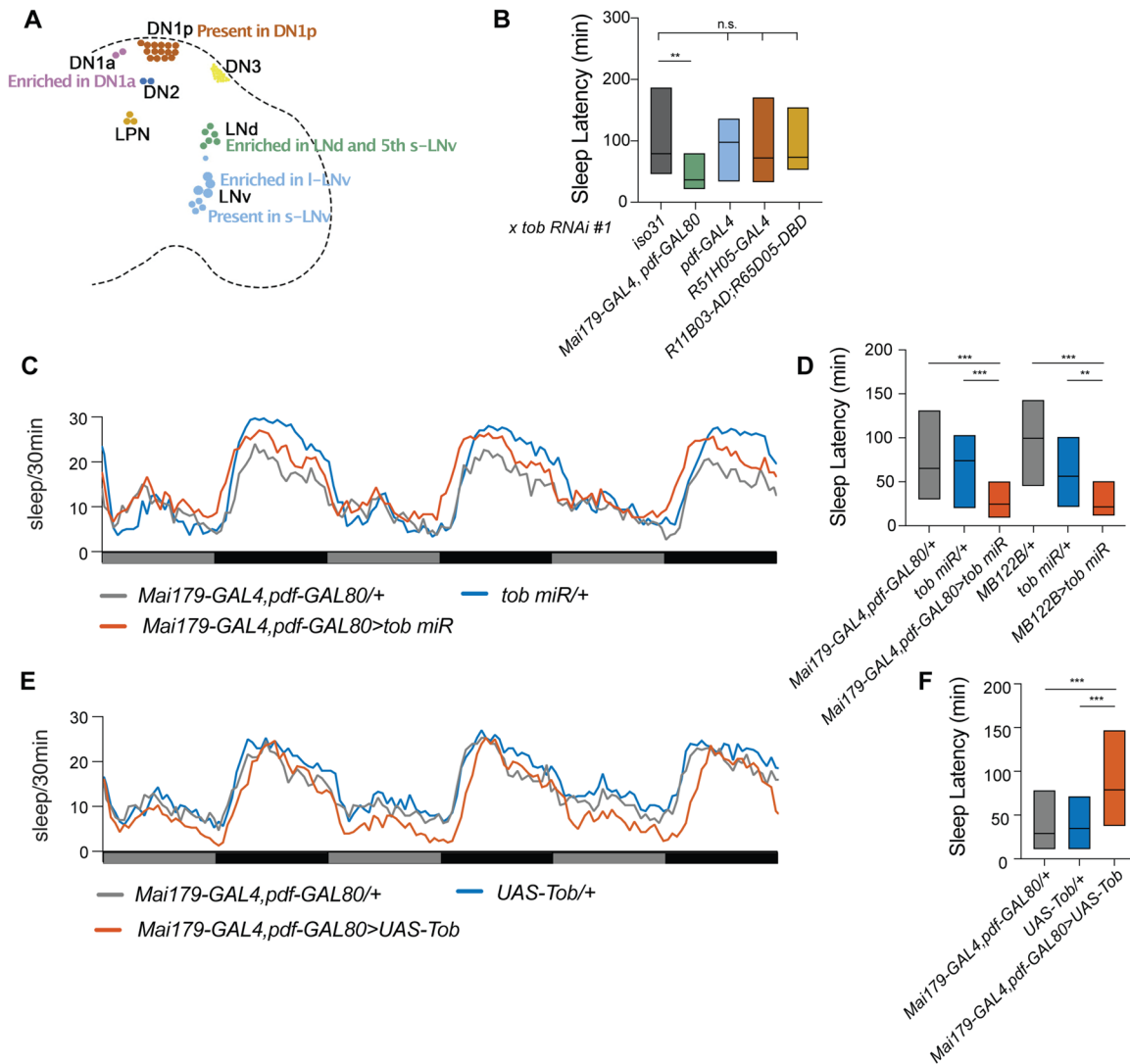


**Figure 4.** Tob acts in evening cells to regulate sleep onset timing at night. **A**, Schematic of fly hemibrain showing clock neuron subpopulations where *tob* mRNA is present or enriched, according to single-cell RNA-seq data (Ma et al., 2021). **B**, Simplified box plots showing sleep onset latency in DD of *tob* knockdown (with *UAS-tob RNAi#1*) using *Mai179-GAL4, pdf-GAL80* (LNd + 5th s-LNv driver, green,  $n = 39$ ), *pdf-GAL4* (LNv driver, blue,  $n = 30$ ), *R51H05-GAL4* (DN1p driver, brown;  $n = 30$ ), *R11B03-AD;R65D05-DBD* (LPN driver, yellow,  $n = 22$ ), and no GAL4 driver (control, gray,  $n = 61$ ). **C**, Sleep profile of *Mai179-GAL4, pdf-GAL80>ctrl* (gray), *ctrl>UAS-tob miR* (blue), and *Mai179-GAL4, pdf-GAL80>UAS-tob miR* (red). **D**, Simplified box plots showing sleep onset latency in DD of *Mai179-GAL4, pdf-GAL80>ctrl* (gray,  $n = 47$ ), *ctrl>UAS-tob miR* (blue,  $n = 45$ ), and *Mai179-GAL4, pdf-GAL80>UAS-tob miR* (red,  $n = 46$ ). **E**, Sleep profile of *Mai179-GAL4, pdf-GAL80>ctrl* (gray), and *ctrl>UAS-tob-tdTomato* (blue), and *Mai179-GAL4, pdf-GAL80>UAS-tob-tdTomato* (red). **F**, Simplified box plots for sleep onset latency in DD of *Mai179-GAL4, pdf-GAL80>ctrl* (gray,  $n = 36$ ), and *ctrl>UAS-tob-tdTomato* (blue,  $n = 38$ ), and *Mai179-GAL4, pdf-GAL80>UAS-tob-tdTomato* (red,  $n = 41$ ). \*\*, \*\*\*, and n.s. denote  $p < 0.01$ ,  $p < 0.001$ , and n.s., respectively.

## Discussion

Sleep is known to be under clock control. However, our knowledge of the molecular mechanisms underlying the circadian control of sleep is limited. Through a large-scale screen of conserved SCN genes, we identify a novel regulator of sleep, Tob, that contributes to the timing of the wake-to-sleep transition. Although flies exhibit bouts of sleep during the day and the night, our data suggest a model where Tob levels cycle under clock control and mediate circadian regulation of sleep onset at night (Fig. 6G). In this model, Tob levels rise during the day in evening cells. This increased Tob expression enhances postsynaptic potentiation in evening cells at dusk and helps maintain the evening peak of activity, thus delaying sleep onset. In contrast, when Tob expression is knocked down in evening cells, synaptic strength is not altered during the dawn but is significantly reduced at dusk, leading to a selective reduction in evening activity and an advanced

sleep onset. Why would the circadian clock need to selectively promote arousal at dusk? One potential reason may be to oppose the increased homeostatic sleep drive at dusk (which is not present at dawn) to enable the crepuscular behavioral patterns seen in flies.

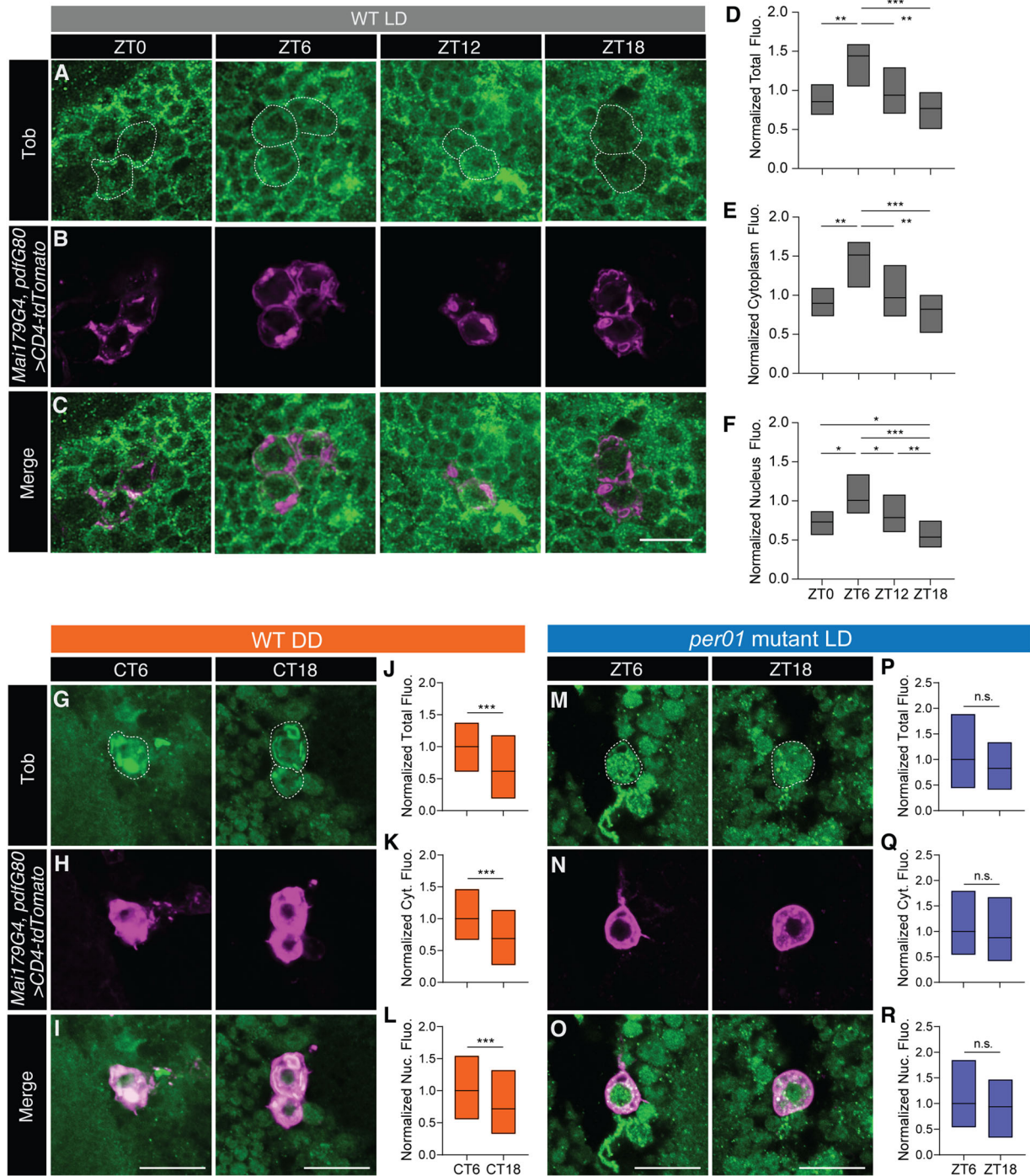
What are the mechanisms by which Tob impacts synaptic strength? Tob is a multifunctional protein that participates in both transcriptional and translational regulation (Yoshida et al., 2000, 2003; Hosoda et al., 2011; White-Grindley et al., 2014). Although Tob molecules function to inhibit cell growth outside of the nervous system (Yoshida et al., 2000, 2003; Hosoda et al., 2011; Ogami et al., 2014), Tob has been shown to regulate synaptic plasticity within the nervous system. In the mammalian hippocampus, Tob is important for memory formation and stress response (Jin et al., 2005; Youssef et al., 2022). In the *Drosophila* mushroom bodies, Tob binds to Orb2, *Drosophila*

Table 4. Additional sleep parameters related to Figure 4

Genotype	LD activity		LD sleep latency (min)		LD day sleep (min)		LD night sleep (min)		LD sleep bout number		LD sleep bout duration (min)	
	Mean ± SEM		Median (25–75%)	Mean ± SEM	Mean ± SEM	Mean ± SEM	Mean ± SEM	Mean ± SEM	Mean ± SEM	Median (25–75%)	Mean ± SEM	Median (25–75%)
<i>Mai179-G4, pdf-G80 &gt; UAS-tob mir</i>	1,289 ± 51.61		21.5 (13.75–33.88)	273.1 ± 10.74	518.4 ± 12.34	16.02 ± 0.69	34.03 (26.16–44.98)					
	$F_{(2,121)} = 0.9627$		$H = 2.466$	$F_{(2,121)} = 4.452$	$F_{(2,121)} = 62.39$	$F_{(2,121)} = 19.59$	$H = 49.96$					
	vs UAS: $p = 0.4359$		vs UAS: $p = 0.9999$	vs UAS: $p = 0.0102$	vs UAS: $p < 0.0001$	vs UAS: $p < 0.0001$	vs UAS: $p < 0.0001$					
<i>UAS-tob mir/+</i>	vs G4: $p = 0.4881$		vs G4: $p > 0.9999$	vs G4: $p = 0.5215$	vs G4: $p = 0.0002$	vs G4: $p = 0.9453$						
	1,373 ± 47.45		17.5 (12.5–30.0)	223.1 ± 12.26	626.2 ± 8.32	10.35 ± 0.83	77.25 (48.95–144.4)					
	1,370 ± 48.39		21.0 (15.75–34.5)	233.9 ± 13.99	454 ± 11.63	15.68 ± 0.62	29.10 (24.78–38.13)					
<i>MB122B-splitG4 &gt; UAS-tob mir</i>	1,269 ± 54.89		23.75 (14.13–40.9)	200 ± 13.98	574.5 ± 11.35	12.82 ± 0.91	49.28 (33.45–108.6)					
	$F_{(2,138)} = 2.354$		$H = 3.086$	$F_{(2,138)} = 2.270$	$F_{(2,138)} = 6.653$	$F_{(2,138)} = 0.1457$	$H = 3.255$					
	vs UAS: $p = 0.2028$		vs UAS: $p = 0.3256$	vs UAS: $p = 0.8431$	vs UAS: $p > 0.9999$	vs UAS: $p = 0.8855$	vs UAS: $p > 0.9999$					
<i>UAS-tob mir/+</i>	vs G4: $p = 0.1159$		vs G4: $p = 0.4740$	vs G4: $p = 0.2863$	vs G4: $p = 0.0052$	vs G4: $p > 0.9999$	vs G4: $p = 0.4525$					
	1,411 ± 58.95		27.5 (19.5–42.0)	210.8 ± 14.71	574.6 ± 9.39	12.28 ± 0.83	55.05 (34.50–90.40)					
	1,436 ± 62.93		30.0 (14.88–44.13)	170.7 ± 12.18	524.1 ± 12.76	12.82 ± 0.68	45.28 (29.15–68.64)					
<i>Mai179-G4, pdf-G80/+</i>	1,596 ± 57.80		38.5 (23.25–57.5)	209.3 ± 16.99	401.9 ± 14.91	14.64 ± 0.56	29.85 (22.55–35.95)					
	$F_{(2,112)} = 9.691$		$H = 6.099$	$F_{(2,112)} = 8.711$	$F_{(2,112)} = 10.47$	$F_{(2,112)} = 5.364$	$H = 12.66$					
	vs UAS: $p = 0.1453$		vs UAS: $p = 0.2160$	vs UAS: $p = 0.3084$	vs UAS: $p < 0.0001$	vs UAS: $p = 0.9211$	vs UAS: $p = 0.0279$					
<i>UAS-tob/+</i>	vs G4: $p < 0.0001$		vs G4: $p = 0.0527$	vs G4: $p = 0.0002$	vs G4: $p = 0.0797$	vs G4: $p = 0.0095$	vs G4: $p > 0.9999$					
	1,218 ± 71.22		28.5 (14.75–38.25)	307 ± 15.09	449.5 ± 17.50	17.91 ± 0.89	24.20 (17.98–36.33)					
	1,436 ± 50.54		27.0 (14.25–47.0)	243.4 ± 17.20	499.4 ± 13.19	15.05 ± 0.78	41.55 (23.98–51.35)					
Genotype	DD activity		DD day sleep (min)		DD night sleep (min)		DD sleep bout number		DD sleep bout duration (min)			
	Mean ± SEM		Mean ± SEM	Mean ± SEM	Mean ± SEM	Mean ± SEM	Mean ± SEM	Mean ± SEM	Median (25–75%)			
<i>Mai179-G4, pdf-G80 &gt; UAS-tob mir</i>	1,479 ± 68.57		236.8 ± 14.96	495.1 ± 12.98	17.30 ± 0.58	30.62 (25.82–36.72)						
	$F_{(2,122)} = 2.303$		$F_{(2,122)} = 0.9287$	$F_{(2,122)} = 39.29$	$F_{(2,122)} = 23.42$	$H = 59.26$						
	vs UAS: $p = 0.5279$		vs UAS: $p = 0.7811$	vs UAS: $p = 0.2957$	vs UAS: $p < 0.0001$	vs UAS: $p < 0.0001$	vs UAS: $p < 0.0001$					
<i>UAS-tob mir/+</i>	vs G4: $p = 0.0851$		vs G4: $p = 0.3637$	vs G4: $p < 0.0001$	vs G4: $p = 0.9691$	vs G4: $p = 0.0017$						
	1,587 ± 71.01		222.3 ± 15.48	523 ± 10.64	11.48 ± 0.77	58.17 (36.38–97.62)						
	1,698 ± 76.79		206.8 ± 16.12	363.1 ± 16.35	17.07 ± 0.69	22.13 (16.1–28.37)						
<i>MB122B-splitG4 &gt; UAS-tob mir</i>	1,339 ± 69.47		202.9 ± 17.38	564.4 ± 0.98	13.89 ± 0.98	49.67 (34.13–101.5)						
	$F_{(2,137)} = 4.212$		$F_{(2,137)} = 3.696$	$F_{(2,137)} = 15.67$	$F_{(2,137)} =$	$H = 5.872$						
	vs UAS: $p = 0.0248$		vs UAS: $p = 0.2357$	vs UAS: $p = 0.002$	vs UAS: $p = 0.0020$	vs UAS: $p = 0.7278$	vs UAS: $p = 0.0108$					
<i>UAS-tob mir/+</i>	vs G4: $p = 0.0518$		vs G4: $p = 0.0213$	vs G4: $p < 0.0001$	vs G4: $p < 0.0001$	vs G4: $p = 0.0462$	vs G4: $p = 0.5311$					
	1,635 ± 75.50		167.2 ± 14.48	499.4 ± 13.61	13.35 ± 0.73	44.50 (32.40–77.13)	vs G4: $p = 0.0095$					
	1,604 ± 91.84		143.6 ± 14.44	460 ± 14.57	13.42 ± 0.78	36.30 (25.89–53.98)	vs G4: $p = 0.0095$					
<i>MB122B-splitG4/+</i>	1,856 ± 109		147.5 ± 17.01	341.5 ± 16.06	16.05 ± 0.83	21.82 (16.0–28.19)	vs G4: $p = 0.0108$					
	$F_{(2,112)} = 13.81$		$F_{(2,112)} = 12.16$	$F_{(2,112)} = 23.49$	$F_{(2,112)} = 2.494$	$H = 8.484$	vs UAS: $p = 0.1325$					
	vs UAS: $p < 0.0001$		vs UAS: $p < 0.0001$	vs UAS: $p < 0.0001$	vs UAS: $p = 0.1345$	vs UAS: $p = 0.0108$	vs UAS: $p = 0.1345$					
<i>Mai179-G4, pdf-G80/+</i>	vs G4: $p = 0.0001$		vs G4: $p = 0.0061$	vs G4: $p = 0.0002$	vs G4: $p = 0.1345$	vs G4: $p = 0.0095$	vs G4: $p = 0.5311$					
	1,342 ± 69.07		229.6 ± 20.36	430.1 ± 15.77	18.36 ± 0.78	25.33 (18.85–29)	vs G4: $p = 0.0095$					
	1,288 ± 69.26		270.8 ± 17.29	483 ± 13.06	18.30 ± 0.85	27.10 (22.25–37.68)	vs G4: $p = 0.0095$					

These data are derived from the dataset shown in Figure 4D and F.

One-way ANOVA with post hoc Tukey used for all variables, except for LD sleep bout duration, and DD sleep bout duration for which Kruskal–Wallis with post hoc Dunn's was used.



**Figure 5.** Tob cycles in evening cells under clock control. **A–F**, Whole-mount brain immunostaining of *Mai179-GAL4, pdf-GAL80>UAS-CD4::tdTomato* flies at ZT0 ( $n = 7$ ), ZT6 ( $n = 6$ ), ZT12 ( $n = 13$ ), and ZT18 ( $n = 15$ ). **G–L**, Whole-mount brain immunostaining of *Mai179-GAL4, pdf-GAL80>UAS-CD4::tdTomato* flies at CT6 ( $n = 22$ ) and CT18 ( $n = 24$ ). **M–R**, Whole-mount brain immunostaining of *Mai179-GAL4, pdf-GAL80>UAS-CD4::tdTomato* flies in the *per<sup>01</sup>* mutant background at ZT6 ( $n = 20$ ) and ZT18 ( $n = 21$ ). Representative images, showing anti-Tob staining in LND neuron cell bodies (white dotted line; **A,G,M**, green); anti-dsRed (**B**, magenta) or anti-RFP staining (**H,N**, magenta); and merged images (**C,I,O**). Simplified box plots showing normalized Tob signal in the cell body (**D,J,P**), cytoplasm (**E,K,Q**), and nucleus (**F,L,R**) of LND neurons. Scale bars in **C** denote 10 mm, and scale bars in **I** and **O** denote 50 mm. \*, \*\*, \*\*\*, and n.s. denote  $p < 0.05$ ,  $p < 0.01$ ,  $p < 0.001$ , and not significant, respectively.

homolog of CPEB2, and enables its amyloid-like oligomerization, which transforms Orb2 from a translation repressor to a translation activator and is critical for formation of long-term courtship memory (White-Grindley et al., 2014; Khan et al., 2015). Thus, Tob may facilitate transcriptional or translational regulation of downstream target genes to modulate neuronal growth/plasticity. The cycling of Tob in a clock-dependent manner may thus

enable a convenient mechanism for the clock to temporally regulate a suite of genes involved in cycling of synaptic strength. The peak of Tob expression in evening cells is earlier than that observed in the l-LNVs and precedes the peak of evening cell  $Ca^{2+}$  activity and the evening activity peak (Fig. 5). In contrast, the physiological and behavioral phenotypes of Tob knockdown are observed at ZT12. This discrepancy suggests that the effects of

**Table 5. Circadian parameters related to manipulation of Tob**

Genotype	Period length (h) Mean ± SEM	Rhythm strength Mean ± SEM	Evening peak phase Mean ± SEM	Biological replicates
<i>nSyb-G4&gt;UAS-tob RNAi #1</i>	24.17 ± 0.04 $F_{(8,379)} = 2.787$ vs UAS: $p = 0.9998$ vs G4: $p = 0.0346$ $n = 42$	0.056 ± 0.006 $F_{(8,425)} = 16.60$ vs UAS: $p = 0.2118$ vs G4: $p < 0.0001$ $n = 44$	10.59 ± 0.188 $F_{(8,558)} = 11.51$ vs UAS: $p < 0.0001$ vs G4: $p < 0.0001$ $n = 44$	3
<i>UAS-tob RNAi #1/+</i>	24.07 ± 0.1 $n = 32$	0.039 ± 0.006 $n = 35$	12.24 ± 0.176 $n = 35$	3
<i>nSyb-G4&gt;UAS-tob RNAi #2</i>	24.41 ± 0.32 vs UAS: $p = 0.9985$ vs G4: $p = 0.8807$ $n = 33$	0.025 ± 0.004 vs UAS: $p < 0.0001$ vs G4: $p > 0.9999$ $n = 42$	11.52 ± 0.185 vs UAS: $p = 0.2145$ vs G4: $p = 0.0054$ $n = 40$	3
<i>UAS-tob RNAi #2/+</i>	24.28 ± 0.06 $n = 46$	0.061 ± 0.005 $n = 46$	12.14 ± 0.151 $n = 61$	3
<i>nSyb-G4&gt;UAS-tob miR</i>	24.14 ± 0.07 vs UAS: $p = 0.9906$ vs G4: $p = 0.0186$ $n = 43$	0.026 ± 0.003 vs UAS: $p = 0.0029$ vs G4: $p > 0.9999$ $n = 46$	11.39 ± 0.160 vs UAS: $p = 0.9469$ vs G4: $p = 0.0002$ $n = 47$	3
<i>UAS-tob miR/+</i>	24.30 ± 0.07 $n = 39$	0.050 ± 0.006 $n = 45$	11.68 ± 0.159 $n = 60$	3
<i>nSyb-G4/+</i>	24.63 ± 0.06 $n = 81$	0.024 ± 0.002 $n = 88$	12.35 ± $n = 116$	3
<i>Mai179-G4,pdf-G80&gt;UAS-tob miR</i>	24.34 ± 0.14 vs UAS: $p > 0.9999$ vs G4: $p > 0.9999$ $n = 42$	0.027 ± 0.003 vs UAS: $p = 0.0037$ vs G4: $p = 0.1357$ $n = 47$	11.74 ± 0.138 vs UAS: $p > 0.9999$ vs G4: $p = 0.3767$ $n = 92$	3
<i>Mai179-G4,pdf-G80/+</i>	24.66 ± 0.27 $n = 30$	0.010 ± 0.002 $n = 41$	12.17 ± 0.146 $n = 72$	3
<i>nSyb-G4&gt;UAS-tob</i>	24.14 ± 0.23 $F_{(2,118)} = 3.340$ vs UAS: $p = 0.411$ vs G4: $p = 0.0293$ $n = 39$	0.02 ± 0.003 $F_{(2,126)} = 10.95$ vs UAS: $p = 0.0405$ vs G4: $p < 0.0001$ $n = 44$	12.28 ± 0.270 $F_{(2,124)} = 0.0751$ vs UAS: $p = 0.9224$ vs G4: $p = 0.9694$ $n = 44$	3
<i>UAS-tob/+</i>	24.48 ± 0.1 $n = 38$	0.03 ± 0.003 $n = 40$	12.17 ± 0.174 $n = 42$	3
<i>nSyb-G4</i>	24.79 ± 0.18 $n = 44$	0.05 ± 0.005 $n = 45$	12.22 ± 0.183 $n = 48$	3
<i>Mai179-G4,pdf-G80&gt;UAS-tob</i>	24.14 ± 0.20 $F_{(2,102)} = 1.619$ vs UAS: $p = 0.4202$ vs G4: $p = 0.1890$ $n = 32$	0.02 ± 0.002 $F_{(2,122)} = 5.70$ vs UAS: $p = 0.0042$ vs G4: $p = 0.6907$ $n = 42$	11.85 ± 0.223 $F_{(2,120)} = 3.831$ vs UAS: $p = 0.4919$ vs G4: $p = 0.2533$ $n = 44$	3
<i>UAS-tob/+</i>	24.53 ± 0.18 $n = 37$	0.03 ± 0.004 $n = 41$	12.20 ± 0.218 $n = 44$	3
<i>Mai179-G4,pdf-G80/+</i>	24.69 ± 0.26 $n = 36$	0.02 ± 0.003 $n = 42$	11.37 ± 0.205 $n = 43$	3

One-way ANOVA with post hoc Tukey used for all variables.

Tob on evening cell function can take hours to manifest, which is consistent with a role in transcription/translation regulation, as well as synaptic plasticity.

In recent years, the discovery of clock output molecules in *Drosophila* has further enriched our understanding of the mechanisms of sleep timing regulation downstream of the core clock, with interesting parallels in mammals (Blum et al., 2018; King and Sehgal, 2020). For example, a transcription factor Mef2 regulates daily plasticity of s-LNv neurons by regulating Fas2 (Sivachenko et al., 2013). Following this discovery in *Drosophila*, mammalian researchers subsequently found that knocking down Mef2D, a mammalian homolog of Mef2, alters the timing of sleep patterns in mice (Mohawk et al., 2019). DH31, the fly homolog of calcitonin gene-related peptide

(CGRP), was previously shown to act in DN1 clock neurons to rhythmically promote wakefulness in the late night (Kunst et al., 2014). In mice, CGRP-expressing brainstem neurons have also been shown to promote arousal, although not specifically in a circadian-dependent manner (Kaur et al., 2017). Additionally, Wide Awake (WAKE) and the E3 ligase Fbx14 are both clock output molecules that regulate GABA<sub>A</sub> receptors in a set of arousal-promoting clock neurons in flies (Liu et al., 2014; Li et al., 2017). Interestingly, mouse WAKE is enriched in the SCN, as well as multiple regions in the hypothalamus and has been recently shown to play a role in rhythmic arousal (Bell et al., 2021; Liu et al., 2023).

Based on our findings, we propose that Tob acts as a clock output molecule that mediates cycling of postsynaptic potentiation in

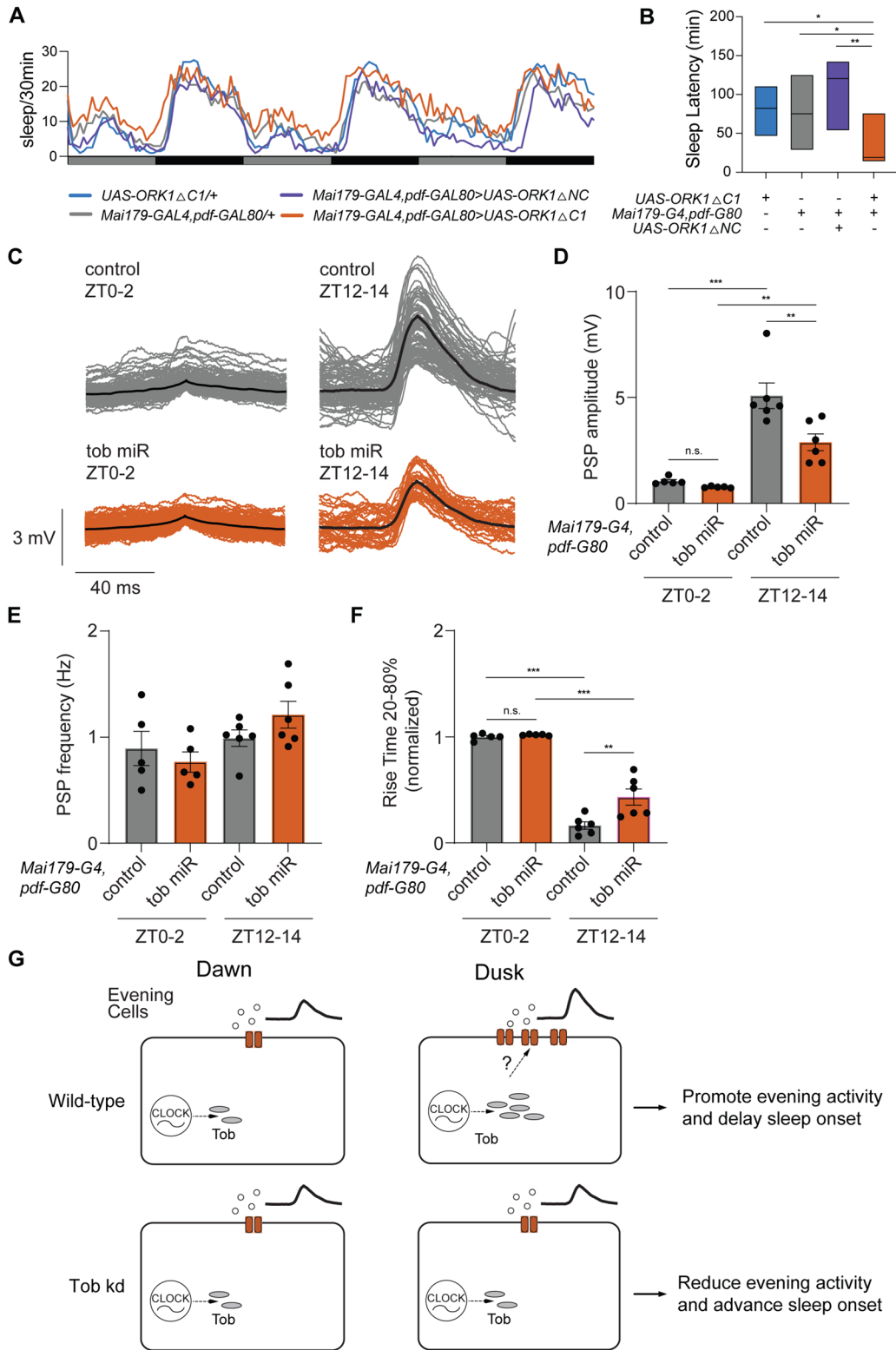


**Figure 6.** Tob regulates postsynaptic potentiation of evening cells. **A**, Sleep profile of *Mai179-GAL4, pdf-GAL80>ctrl* (gray), *ctrl>UAS-ORK1DNC* (blue), *Mai179-GAL4, pdf-GAL80>UAS-ORK1DNC* (purple), and *Mai179-GAL4, pdf-GAL80>UAS-ORK1DNC* (red). **B**, Simplified box plots showing sleep onset latency of *Mai179-GAL4, pdf-GAL80>ctrl* (gray,  $n = 27$ ), *ctrl>UAS-ORK1DNC* (blue,  $n = 29$ ), *Mai179-GAL4, pdf-GAL80>UAS-ORK1DNC* (purple,  $n = 22$ ), and *Mai179-GAL4, pdf-GAL80>UAS-ORK1DNC* (red,  $n = 12$ ). **C**, Superimposed membrane potential traces for spontaneous PSPs of LNd neurons from *Mai179-GAL4, pdf-GAL80>UAS-mCD8::GFP* flies in the presence (red,  $n = 5, 6$ ) and absence (gray,  $n = 5, 6$ ) of *tob miR* at ZT0-2 or ZT12-14, respectively. **D-F**, Amplitude (**D**), frequency (**E**), and 20–80% rise time (normalized based on mean value of controls; **F**) of spontaneous PSPs from the flies in **C**. \*, \*\*, \*\*\*, and n.s. denote  $p < 0.05$ ,  $p < 0.01$ ,  $p < 0.0001$ , and not significant, respectively. **G**, Model of Tob promoting circadian clock regulation of sleep onset at night in evening cells. Tob expression is under clock control, with higher levels in the afternoon. Tob promotes postsynaptic potentiation in evening cells at dusk. This postsynaptic potentiation of evening cells facilitates maintenance of evening activity, delaying sleep onset at night. Knockdown of Tob in evening cells leads to reduced postsynaptic potentiation of evening cells specifically at dusk, decreasing evening activity and advancing sleep onset at night.

LNds in the evening, which is important for maintaining evening activity and delaying sleep onset. Given the rhythmic expression of Tob1 in the SCN, and existing knowledge of daily plasticity mechanisms in the SCN (Girardet et al., 2010), the study of Tob in mammals might shed light on similar processes in the SCN.

## References

- Allada R, Chung BY (2010) Circadian organization of behavior and physiology in *Drosophila*. *Annu Rev Physiol* 72:605–624.
- Allada R, Siegel JM (2008) Unearthing the phylogenetic roots of sleep. *Curr Biol* 18:R670–R679.
- Bedont JL, et al. (2017) An LHX1-regulated transcriptional network controls sleep/wake coupling and thermal resistance of the central circadian clockworks. *Curr Biol* 27:128–136.
- Bell BJ, Wang AA, Kim DW, Xiong J, Blackshaw S, Wu MN (2021) Characterization of *mWake* expression in the murine brain. *J Comp Neurol* 529:1954–1987.
- Blum ID, Bell B, Wu MN (2018) Time for bed: genetic mechanisms mediating the circadian regulation of sleep. *Trends Genet* 34:379–388.
- Borbély AA, Daan S, Wirz-Justice A, Deboer T (2016) The two-process model of sleep regulation: a reappraisal. *J Sleep Res* 25:131–143.
- Chen C-H, Huang H, Ward CM, Su JT, Schaeffer LV, Guo M, Hay BA (2007) A synthetic maternal-effect selfish genetic element drives population replacement in *Drosophila*. *Science* 316:597–600.
- Cheng MY, Bullock CM, Li C, Lee AG, Bermak JC, Belluzzi J, Weaver DR, Leslie FM, Zhou Q-Y (2002) Prokineticin 2 transmits the behavioural circadian rhythm of the suprachiasmatic nucleus. *Nature* 417:405–410.
- Collins B, et al. (2020) Circadian VIPergic neurons of the suprachiasmatic nuclei sculpt the sleep–wake cycle. *Neuron* 108:486–499.e5.
- Dijk D-J, Lockett SW (2002) Invited review: integration of human sleep–wake regulation and circadian rhythmicity. *J Appl Physiol* 92:852–862.
- Dubowy C, Sehgal A (2017) Circadian rhythms and sleep in *Drosophila melanogaster*. *Genetics* 205:1373–1397.
- Girardet C, Blanchard M-P, Ferracci G, Lévêque C, Moreno M, François-Bellan A-M, Becquet D, Bosler O (2010) Daily changes in synaptic innervation of VIP neurons in the rat suprachiasmatic nucleus: contribution of glutamatergic afferents. *Eur J Neurosci* 31:359–370.
- Guo F, Cerullo I, Chen X, Rosbash M (2014) PDF neuron firing phase-shifts key circadian activity neurons in *Drosophila*. *eLife* 3:e02780.
- Herzog ED, Hermansteyne T, Smyllie NJ, Hastings MH (2017) Regulating the suprachiasmatic nucleus (SCN) circadian clockwork: interplay between cell-autonomous and circuit-level mechanisms. *Cold Spring Harbor Perspect Biol* 9:a027706.
- Hosoda N, Funakoshi Y, Hirasawa M, Yamagishi R, Asano Y, Miyagawa R, Ogami K, Tsujimoto M, Hoshino S (2011) Anti-proliferative protein Tob negatively regulates CPEB3 target by recruiting Caf1 deadenylation: tob regulates deadenylation of CPEB3 target. *EMBO J* 30:1311–1323.
- Irish LA, Kline CE, Gunn HE, Buysse DJ, Hall MH (2015) The role of sleep hygiene in promoting public health: a review of empirical evidence. *Sleep Med Rev* 22:23–36.
- Jagannath A, Peirson SN, Foster RG (2013) Sleep and circadian rhythm disruption in neuropsychiatric illness. *Curr Opin Neurobiol* 23:888–894.
- Jagannath A, Taylor L, Wakaf Z, Vasudevan SR, Foster RG (2017) The genetics of circadian rhythms, sleep and health. *Hum Mol Genet* 26:R128–R138.
- Jin M, et al. (2005) The negative cell cycle regulator, Tob (transducer of ErbB-2), is a multifunctional protein involved in hippocampus-dependent learning and memory. *Neuroscience* 131:647–659.
- Joiner WJ, Crocker A, White BH, Sehgal A (2006) Sleep in *Drosophila* is regulated by adult mushroom bodies. *Nature* 441:757–760.
- Kalsbeek A, Perreau-Lenz S, Buijs RM (2006) A network of (autonomic) clock outputs. *Chronobiol Int* 23:521–535.
- Kaur S, et al. (2017) A genetically defined circuit for arousal from sleep during hypercapnia. *Neuron* 96:1153–1167.
- Kawamura-Tsuzuku J, Suzuki T, Yoshida Y, Yamamoto T (2004) Nuclear localization of Tob is important for regulation of its antiproliferative activity. *Oncogene* 23:6630–6638.
- Keene AC, Duboue ER (2018) The origins and evolution of sleep. *J Exp Biol* 221:jeb159533.
- Keller A, Sweeney ST, Zars T, O’Kane CJ, Heisenberg M (2002) Targeted expression of tetanus neurotoxin interferes with behavioral responses to sensory input in *Drosophila*. *J Neurobiol* 50:221–233.
- Khan MR, Li L, Pérez-Sánchez C, Saraf A, Florens L, Slaughter BD, Unruh JR, Si K (2015) Amyloidogenic oligomerization transforms *Drosophila* Orb2 from a translation repressor to an activator. *Cell* 163:1468–1483.
- King AN, Sehgal A (2020) Molecular and circuit mechanisms mediating circadian clock output in the *Drosophila* brain. *Eur J Neurosci* 51:268–281.
- Kunst M, Hughes ME, Raccuglia D, Felix M, Li M, Barnett G, Duah J, Nitabach MN (2014) Calcitonin gene-related peptide neurons mediate sleep-specific circadian output in *Drosophila*. *Curr Biol* 24:2652–2664.
- Lavie P (2001) Sleep–wake as a biological rhythm. *Annu Rev Psychol* 52:277–303.
- Li Q, Li Y, Wang X, Qi J, Jin X, Tong H, Zhou Z, Zhang ZC, Han J (2017) *Fbxl4* serves as a clock output molecule that regulates sleep through promotion of rhythmic degradation of the GABAA receptor. *Curr Biol* 27:3616–3625.e5.
- Liu S, et al. (2014) WIDE AWAKE mediates the circadian timing of sleep onset. *Neuron* 82:151–166.
- Liu Q, et al. (2023) A clock-dependent brake for rhythmic arousal in the dorsomedial hypothalamus. *Nat Commun* 14:6381.
- Liu S, Liu Q, Tabuchi M, Wu MN (2016) Sleep drive is encoded by neural plastic changes in a dedicated circuit. *Cell* 165:1347–1360.
- Ma D, Przybylski D, Abruzzi KC, Schlichting M, Li Q, Long X, Rosbash M (2021) A transcriptomic taxonomy of *Drosophila* circadian neurons around the clock. *eLife* 10:e63056.
- Mistlberger RE (2005) Circadian regulation of sleep in mammals: role of the suprachiasmatic nucleus. *Brain Res Rev* 49:429–454.
- Mohawk JA, Cox KH, Sato M, Yoo S-H, Yanagisawa M, Olson EN, Takahashi JS (2019) Neuronal myocyte-specific enhancer factor 2D (MEF2D) is required for normal circadian and sleep behavior in mice. *J Neurosci* 39:7958–7967.
- Nguyen DL, Hutson AN, Zhang Y, Daniels SD, Peard AR, Tabuchi M (2022) Age-related unstructured spike patterns and molecular localization in *Drosophila* circadian neurons. *Front Physiol* 13:845236.
- Nicholson L, Singh GK, Osterwalder T, Roman GW, Davis RL, Keshishian H (2008) Spatial and temporal control of gene expression in *Drosophila* using the inducible GeneSwitch GAL4 system. I. Screen for larval nervous system drivers. *Genetics* 178:215–234.
- Ogami K, Hosoda N, Funakoshi Y, Hoshino S (2014) Antiproliferative protein Tob directly regulates c-myc proto-oncogene expression through cytoplasmic polyadenylation element-binding protein CPEB. *Oncogene* 33:55–64.
- Panda S, Antoch MP, Miller BH, Su AI, Schook AB, Straume M, Schultz PG, Kay SA, Takahashi JS, Hogenesch JB (2002) Coordinated transcription of key pathways in the mouse by the circadian clock. *Cell* 109:307–320.
- Pembroke WG, Babbs A, Davies KE, Ponting CP, Oliver PL (2015) Temporal transcriptomics suggest that twin-peaking genes reset the clock. *eLife* 4:e10518.
- Persons JL, Abhilash L, Lopatkin AJ, Roelofs A, Bell EV, Fernandez MP, Shafer OT (2022) PHASE, an open-source program for the analysis of *Drosophila* phase, activity, and sleep under entrainment. *J Biol Rhythms* 37:455–467.
- Ryder E, et al. (2004) The DrosDel collection. *Genetics* 167:797–813.
- Sanchez REA, de la Iglesia HO (2021) Sleep and the circadian system: the latest gossip on a tumultuous long-term relationship. *Neurobiol Sleep Circadian Rhythms* 10:100061.
- Sanchez REA, Kalume F, de la Iglesia HO (2022) Sleep timing and the circadian clock in mammals: past, present and the road ahead. *Semin Cell Dev Biol* 126:3–14.
- Shafer OT, Keene AC (2021) The regulation of *Drosophila* sleep. *Curr Biol* 31:R38–R49.
- Shaw PJ, Cirelli C, Greenspan RJ, Tononi G (2000) Correlates of sleep and waking in *Drosophila melanogaster*. *Science* 287:1834–1837.
- Sivachenko A, Li Y, Abruzzi KC, Rosbash M (2013) The transcription factor *Mef2* links the *Drosophila* core clock to *Fas2*, neuronal morphology, and circadian behavior. *Neuron* 79:281–292.
- Suzuki T (2002) Phosphorylation of three regulatory serines of Tob by Erk1 and Erk2 is required for Ras-mediated cell proliferation and transformation. *Genes Dev* 16:1356–1370.

- Takahashi JS, Hong H-K, Ko CH, McDearmon EL (2008) The genetics of mammalian circadian order and disorder: implications for physiology and disease. *Nat Rev Genet* 9:764–775.
- Tang M, et al. (2022) An extra-clock ultradian brain oscillator sustains circadian timekeeping. *Sci Adv* 8:eabo5506.
- Welsh DK, Takahashi JS, Kay SA (2010) Suprachiasmatic nucleus: cell autonomy and network properties. *Annu Rev Physiol* 72:551–577.
- White-Grindley E, Li L, Mohammad Khan R, Ren F, Saraf A, Florens L, Si K (2014) Contribution of Orb2A stability in regulated amyloid-like oligomerization of *Drosophila* Orb2. *PLoS Biol* 12:e1001786.
- Yoshida Y, et al. (2000) Negative regulation of BMP/smad signaling by tob in osteoblasts. *Cell* 103:1085–1097.
- Yoshida Y, von Bubnoff A, Ikematsu N, Blitz IL, Tsuzuku JK, Yoshida EH, Umemori H, Miyazono K, Yamamoto T, Cho K W Y (2003) Tob proteins enhance inhibitory Smad-receptor interactions to repress BMP signaling. *Mech Dev* 120:629–637.
- Youssef MMM, Hamada HT, Lai ESK, Kiyama Y, El-Tabbal M, Kiyonari H, Nakano K, Kuhn B, Yamamoto T (2022) TOB is an effector of the hippocampus-mediated acute stress response. *Transl Psychiatry* 12:302.